SIAM J. SCI. COMPUT.
Vol. 39, No. 4, pp. A1531–A1557

A LEAST-SQUARES-BASED WEAK GALERKIN FINITE ELEMENT METHOD FOR SECOND ORDER ELLIPTIC EQUATIONS*

LIN MU†, JUNPING WANG‡, AND XIU YE§

Abstract. In this article, we introduce a least-squares-based weak Galerkin finite element method for the second order elliptic equation. This new method is shown to provide very accurate numerical approximations for both the primal and the flux variables. In contrast to other existing least-squares finite element methods, this new method allows us to use discontinuous approximating functions on finite element partitions consisting of arbitrary polygon/polyhedron shapes. We also develop a Schur complement algorithm for the resulting discretization problem by eliminating all the unknowns that represent the solution information in the interior of each element. Optimal order error estimates for both the primal and the flux variables are established. An extensive set of numerical experiments are conducted to demonstrate the robustness, reliability, flexibility, and accuracy of the least-squares-based weak Galerkin finite element method. The numerical examples cover a wide range of applied problems, including singularly perturbed reaction-diffusion equations and the flow of fluid in porous media with strong anisotropy and heterogeneity.

Key words. weak Galerkin, finite element methods, least-squares finite element methods, second order elliptic problems

AMS subject classifications. Primary, 65N15, 65N30, 76D07; Secondary, 35B45, 35J50

DOI. 10.1137/16M1083244

1. Introduction.

The least-squares finite element method is a general discretization technique in numerical partial differential equations. The method receives its name by minimizing the residuals in a least-squares fashion. Therefore, a straightforward advantage of the least-squares finite element method is that the resulting linear systems are symmetric and positive definite. Least-squares finite element methods have been developed for the second order elliptic problems in [5, 10, 13, 14, 22, 30],

*Submitted to the journal's Methods and Algorithms for Scientific Computing section July 6, 2016; accepted for publication (in revised form) June 7, 2017; published electronically August 17, 2017.

http://www.siam.org/journals/sisc/39-4/M108324.html

Funding: The first author's work was partially supported by the Householder Fellowship funded by the U.S. Department of Energy, Office of Science, Office of Advanced Scientific Computing Research, Applied Mathematics program, under contract number ERKJE45. This material is based upon work supported by the U.S. Department of Energy, Office of Science, Office of Advanced Scientific Computing Research. This manuscript has been authored by UT-Battelle, LLC under contract DE-AC05-00OR22725 with the U.S. Department of Energy. The United States Government retains and the publisher, by accepting the article for publication, acknowledges that the United States Government retains a non-exclusive, paid-up, irrevocable, world-wide license to publish or reproduce the published form of this manuscript, or allow others to do so, for United States Government purposes. The Department of Energy will provide public access to these results of federally sponsored research in accordance with the DOE Public Access Plan (http://energy.gov/downloads/doe-public-access-plan). The second author's work was supported by the NSF IR/D program, while working at the Foundation. However, any opinion, finding, and conclusions or recommendations expressed in this material are those of the author and do not necessarily reflect the views of the National Science Foundation. The third author's work was supported in part by National Science Foundation grant DMS-1620016.

†Computer Science and Mathematics Division, Oak Ridge National Laboratory, Oak Ridge, TN 37831 (mul1@ornl.gov).

‡Division of Mathematical Sciences, National Science Foundation, Arlington, VA 22230 (jwang@nsf.gov).

§Department of Mathematics, University of Arkansas at Little Rock, Little Rock, AR 72204 (xxye@ualr.edu).

for the Stokes and Navier–Stokes equations in [3, 4, 6, 11, 15, 23], and for elasticity in [12, 28] and references therein. However, due to the consistency requirement, most of the existing least-squares finite element methods have limitations in the selection of approximation functions and the underlying finite element partitions.

Using discontinuous approximations in finite element procedure provides flexibility in mesh generation and the construction of finite element functions. The research of finite element methods with discontinuous approximations has received extensive attention in the past two decades. Thousands of papers have been published on discontinuous Galerkin techniques. A few representatives include the interior penalty discontinuous Galerkin method [1], the local discontinuous Galerkin method [17], the hybridizable discontinuous Galerkin method [16], the mimetic finite differences [2], the mix finite element method [8], the hybrid high-order methods [32, 31]; see also the references therein. The weak Galerkin method introduced in [36, 37] is a new finite element procedure that makes use of discontinuous polynomials on polytopal mesh.

Least-squares finite element methods with discontinuous approximation have been investigated in recent years. Discontinuous Galerkin (DG) least-squares methods have been developed in [6, 7] for solving the Stokes equations in velocity-vorticity-pressure form. These DG least-squares methods are locally conservative to prevent nonphysical solutions. Optimal or near-optimal convergence rates of the methods are confirmed numerically. Some first order DG least-squares methods [26, 27] have been developed for singularly perturbed reaction-diffusion problems. Another finite element method closely related to the DG least-squares method is the DPG method [18, 19], since it can be viewed as applying the least-squares method to a preconditioned system. The DPG method has its name by using discontinuous approximation in Petrov–Galerkin formulation with optimal testing function.

In this paper, we develop a weak Galerkin least-squares finite element method for the second order elliptic equation and prove optimal order error estimates for both the primal and the flux variables. Compared with the conforming first order system least-squares method, the weak Galerkin least-squares method has the advantages of easy construction of high-order elements and allowing general polytope meshes with hanging nodes. Such features have been confirmed by our numerical examples. The weak Galerkin least-squares method has advantages over standard DG methods by guaranteeing a symmetric positive definite and parameter-independent system and providing accurate approximations for both the primal and the flux variables. One unique feature of the weak Galerkin least-squares method is that globally coupled unknowns are those defined only on element boundaries. This makes the weak Galerkin least-squares method computationally efficient compared with DG least-squares methods.

An extensive set of numerical experiments was conducted and reported in order to demonstrate the potential of this new method in scientific computing. In particular, we believe that the least-squares-based weak Galerkin finite element method offers an efficient and reliable numerical technique for singularly perturbed reaction-diffusion equations with strong anisotropy and heterogeneity in porous media, as applied to the computation of Darcy flows.

The model problem considered in this paper seeks an unknown function u satisfying

$$-\nabla \cdot (a\nabla u) + cu = f \quad \text{in } \Omega, \tag{1.1}$$

$$u = g \quad \text{on } \partial\Omega, \tag{1.2}$$

where $c \geq 0$ and Ω is a polytopal domain in $\mathbb{R}^d$ (polygonal or polyhedral domain [35] for $d = 2, 3$), ∇u denotes the gradient of the function u, and a is a $d \times d$ tensor that is uniformly bounded and symmetric positive definite in the domain. The partial differential equation (1.1) has a wide range of applications in science and engineering, and it is a benchmark testing problem for new discretization techniques. The problem (1.1)–(1.2) has an equivalent formulation in mixed form: Find $\mathbf{q} = \mathbf{q}(\mathbf{x})$ and $u = u(\mathbf{x})$ satisfying

$$\mathbf{q} + a\nabla u = 0 \quad \text{in } \Omega, \tag{1.3}$$

$$\nabla \cdot \mathbf{q} + cu = f \quad \text{in } \Omega, \tag{1.4}$$

$$u = g \quad \text{on } \partial\Omega. \tag{1.5}$$

In this paper, we shall provide all the details and basic ideas of the least-squares-based weak Galerkin finite element method for the system of linear equations (1.3)–(1.5). This approach and the underlying basic principle can be adapted to other partial differential equations in general.

In application to earth science problems, the system (1.3)–(1.4), with $c = 0$, may be used to describe the flow of fluid in porous media where (1.3) is known as Darcy's law and (1.4) arises from mass conservation. The tensor a represents the permeability of the porous media. The unknown function $\mathbf{q}$ is the velocity/flux variable, and u is the hydraulic pressure. In section 6, we shall present some numerical results with a focus on fluid flow problems where the porous media has strong anisotropy and heterogeneity. Our numerical experiments indicate that the least-squares-based weak Galerkin method is capable of providing very accurate numerical approximations for both the pressure and the velocity/flux variables simultaneously. In section 7, we consider singularly perturbed reaction-diffusion problems, namely, (1.1), in which the coefficient $a = \epsilon^2$ is very small. It is well known that the development of robust and reliable numerical schemes for such systems is challenging when ϵ is very small. Our numerical experiments indicate that the least-squares-based weak Galerkin method has great potential for singularly perturbed reaction-diffusion problems.

2. Weak Galerkin least-squares method. Let $\mathcal{T}_h$ be a partition of the domain Ω consisting of polygons in two dimension or polyhedra in three dimension that are shape-regular according to the conditions specified in [37]. Denote by $\mathcal{E}_h$ the set of all edges or flat faces in $\mathcal{T}_h$, and let $\mathcal{E}_h^0 = \mathcal{E}_h \backslash \partial\Omega$ be the set of all interior edges or flat faces. For every element $T \in \mathcal{T}_h$, we denote by h_T its diameter and mesh size $h = \max_{T\in\mathcal{T}_h} h_T$ for $\mathcal{T}_h$.

The weak Galerkin method takes finite element functions in the form of two components—one in the interior and the other on the boundary:

$$v = \begin{cases} v_0 & \text{in } T, \\ v_b & \text{on } \partial T. \end{cases}$$

For simplicity, we write v as $v = \{v_0, v_b\}$ for short.

For convenience, we introduce a set of normal directions on $\mathcal{E}_h$ as follows:

$$\mathcal{D}_h = \{\mathbf{n}_e : \ \mathbf{n}_e \text{ is unit and normal to } e, \ e \in \mathcal{E}_h\}. \tag{2.1}$$

We now introduce two finite element spaces: V_h for the pressure variable u and Σ_h for the flux variable $\mathbf{q}$, defined as follows:

$$V_h = \{v = \{v_0, v_b\} : \ v_0|_T \in P_{k+1}(T), v_b|_e \in P_k(e), e \subset \partial T\},$$
$$\Sigma_h = \{\boldsymbol{\sigma} = \{\boldsymbol{\sigma}_0, \boldsymbol{\sigma}_b\} : \ \boldsymbol{\sigma}_0|_T \in [P_k(T)]^d, \boldsymbol{\sigma}_b|_e = \sigma_b \mathbf{n}_e, \sigma_b|_e \in P_k(e), \ e \subset \partial T\},$$

where $k \geq 0$ is any nonnegative integer. Let V_h^0 be the subspace of V_h consisting of finite element functions with vanishing boundary value

$$V_h^0 = \{v \in V_h : \ v_b = 0 \text{ on } \partial\Omega\}.$$

ALGORITHM 2.1. *The weak Galerkin least-squares method for the problem* (1.3)–(1.5) *seeks* $u_h = \{u_0, u_b\} \in V_h$ *and* $\mathbf{q}_h = \{\mathbf{q}_0, \mathbf{q}_b\} \in \Sigma_h$ *satisfying* $u_b = Q_b g$ *on* $\partial\Omega$ *and*

$$a(\mathbf{q}_h, u_h; \boldsymbol{\sigma}, v) = (f, \ \nabla_w \cdot \boldsymbol{\sigma} + cv_0) \quad \forall \boldsymbol{\sigma} \times v \in \Sigma_h \times V_h^0. \tag{2.2}$$

The rest of this section shall provide a detailed interpretation for the finite element scheme (2.2). First of all, for any $\boldsymbol{\sigma} = \{\boldsymbol{\sigma}_0, \boldsymbol{\sigma}_b\} \in \Sigma_h$, the discrete weak divergence $\nabla_w \cdot \boldsymbol{\sigma}$ is a piecewise polynomial of degree k satisfying

$$(\nabla_w \cdot \boldsymbol{\sigma}, \phi)_T = -(\boldsymbol{\sigma}_0, \nabla\phi)_T + \langle \boldsymbol{\sigma}_b \cdot \mathbf{n}, \phi\rangle_{\partial T} \qquad \forall \phi \in P_k(T). \tag{2.3}$$

Second, for any $v = \{v_0, v_b\} \in V_h$, the discrete weak gradient $\nabla_w v \in [P_k(T)]^d$ is defined by the equation

$$(\nabla_w v, \tau)_T = -(v_0, \ \nabla \cdot \tau)_T + \langle v_b, \ \tau \cdot \mathbf{n}\rangle_{\partial T} \qquad \forall \tau \in [P_k(T)]^d. \tag{2.4}$$

For any $\kappa = \kappa(x) \geq 0$, denote by

$$(\phi, \psi)_{T,\kappa} = \int_T \kappa(x)\phi\psi dx$$

the κ-weighted L^2 inner product. The corresponding weighted norm is denoted by $\|\phi\|_{T,\kappa} = (\phi, \phi)_{T,\kappa}^{1/2}$.

The bilinear form $a(\boldsymbol{\tau}, w; \boldsymbol{\sigma}, v)$ used in the numerical scheme (2.2) is given by

$$\begin{aligned} a(\boldsymbol{\tau}, w; \boldsymbol{\sigma}, v) = \sum_{T\in\mathcal{T}_h} & ((\nabla_w \cdot \boldsymbol{\tau} + cw_0, \ \nabla_w \cdot \boldsymbol{\sigma} + cv_0)_T \\ & + (\boldsymbol{\tau}_0 + a\nabla_w w, \ \boldsymbol{\sigma}_0 + a\nabla_w v)_{T,a^{-1}}) + s_1(w, v) + s_2(\boldsymbol{\tau}, \boldsymbol{\sigma}), \end{aligned} \tag{2.5}$$

where

$$\begin{aligned} s_1(w, v) &= \sum_{T\in\mathcal{T}_h} h^{-1}\langle Q_b w_0 - w_b, \ Q_b v_0 - v_b\rangle_{\partial T}, \\ s_2(\boldsymbol{\tau}, \boldsymbol{\sigma}) &= \sum_{T\in\mathcal{T}_h} h\langle(\boldsymbol{\tau}_0 - \boldsymbol{\tau}_b)\cdot\mathbf{n}, \ (\boldsymbol{\sigma}_0 - \boldsymbol{\sigma}_b)\cdot\mathbf{n}\rangle_{\partial T}, \end{aligned}$$

and Q_b is the usual L^2 projection from $L^2(e)$ to $P_k(e)$ on each edge $e \subset \partial T$.

3. Solution existence and uniqueness. For simplicity, assume that the coefficients a and c in (1.1) are piecewise constants with respect to the finite element partition $\mathcal{T}_h$. The results in this paper can be extended to variable coefficients without any difficulty, provided that a and c are piecewise smooth.

Introduce a seminorm $|||\cdot|||_V$ in V_h and a seminorm $|||\cdot|||_\Sigma$ in Σ_h as follows:

$$\begin{aligned} |||v|||_V^2 &= \sum_{T\in\mathcal{T}_h} \|\nabla_w v\|_{T,a}^2 + s_1(v, v), \\ |||\boldsymbol{\sigma}|||_\Sigma^2 &= \sum_{T\in\mathcal{T}_h} \|\nabla_w \cdot \boldsymbol{\sigma}\|_T^2 + \|\boldsymbol{\sigma}_0\|_{a^{-1}}^2 + s_2(\boldsymbol{\sigma}, \boldsymbol{\sigma}). \end{aligned}$$

It is not hard to see that $|\!|\!| \cdot |\!|\!|_V$ and $|\!|\!| \cdot |\!|\!|_\Sigma$ defines norms in V_h^0 and Σ_h, respectively.

The following discrete Poincaré inequality has been established in [29]:

$$\|v_0\| \le C|\!|\!|v|\!|\!|_V, \qquad v \in V_h^0. \tag{3.1}$$

LEMMA 3.1. *There exists a constant C such that for all $\boldsymbol{\sigma} \times v \in \Sigma_h \times V_h^0$ one has*

$$a(\boldsymbol{\sigma}, v; \boldsymbol{\sigma}, v) \ge C(|\!|\!|\boldsymbol{\sigma}|\!|\!|_\Sigma^2 + |\!|\!|v|\!|\!|_V^2). \tag{3.2}$$

Proof. First, note that

$$s_1(v, v) \le a(\boldsymbol{\sigma}, v; \boldsymbol{\sigma}, v), \tag{3.3}$$

$$s_2(\boldsymbol{\sigma}, \boldsymbol{\sigma}) \le a(\boldsymbol{\sigma}, v; \boldsymbol{\sigma}, v). \tag{3.4}$$

From (2.3), (2.4), and the definition of Q_b we have

$$\begin{aligned}
-\sum_{T\in\mathcal{T}_h} (\nabla_w v,\ \boldsymbol{\sigma}_0)_T &= \sum_{T\in\mathcal{T}_h} ((v_0,\ \nabla\cdot\boldsymbol{\sigma}_0)_T - \langle v_b,\ \boldsymbol{\sigma}_0\cdot\mathbf{n}\rangle_{\partial T}) \\
&= \sum_{T\in\mathcal{T}_h} (-(\nabla v_0,\ \boldsymbol{\sigma}_0)_T + \langle v_0 - v_b,\ \boldsymbol{\sigma}_0\cdot\mathbf{n}\rangle_{\partial T}) \\
&= \sum_{T\in\mathcal{T}_h} (-(\nabla v_0,\ \boldsymbol{\sigma}_0)_T + \langle \boldsymbol{\sigma}_b\cdot\mathbf{n},\ v_0\rangle_{\partial T} \\
&\quad - \langle v_0 - v_b,\ \boldsymbol{\sigma}_b\cdot\mathbf{n}\rangle_{\partial T} + \langle v_0 - v_b,\ \boldsymbol{\sigma}_0\cdot\mathbf{n}\rangle_{\partial T}) \\
&= \sum_{T\in\mathcal{T}_h} ((\nabla_w\cdot\boldsymbol{\sigma} + cv_0,\ v_0)_T - c(v_0,\ v_0)_T \\
&\quad + \langle v_0 - v_b,\ (\boldsymbol{\sigma}_0 - \boldsymbol{\sigma}_b)\cdot\mathbf{n}\rangle_{\partial T}).
\end{aligned} \tag{3.5}$$

Equation (3.5) gives rise to

$$\begin{aligned}
\sum_{T\in\mathcal{T}_h} \|\nabla_w v\|_{T,a}^2 &= \sum_{T\in\mathcal{T}_h} ((a\nabla_w v + \boldsymbol{\sigma}_0,\ \nabla_w v)_T - (\boldsymbol{\sigma}_0,\ \nabla_w v)_T) \\
&= \sum_{T\in\mathcal{T}_h} ((a\nabla_w v + \boldsymbol{\sigma}_0,\ \nabla_w v)_T + (\nabla_w\cdot\boldsymbol{\sigma} + cv_0,\ v_0)_T - c(v_0,\ v_0)_T \\
&\quad + \langle Q_b v_0 - v_b,\ (\boldsymbol{\sigma}_0 - \boldsymbol{\sigma}_b)\cdot\mathbf{n}\rangle_{\partial T}) \\
&\le \sum_{T\in\mathcal{T}_h} ((a\nabla_w v + \boldsymbol{\sigma}_0,\ \nabla_w v)_T + (\nabla_w\cdot\boldsymbol{\sigma} + cv_0,\ v_0)_T \\
&\quad + \langle Q_b v_0 - v_b,\ (\boldsymbol{\sigma}_0 - \boldsymbol{\sigma}_b)\cdot\mathbf{n}\rangle_{\partial T}) \\
&\le C\left(\sum_{T\in\mathcal{T}_h} (\|a\nabla_w v + \boldsymbol{\sigma}_0\|_{T,a^{-1}}\|\nabla_w v\|_{T,a} + \|\nabla_w\cdot\boldsymbol{\sigma} + cv_0\|_T\|v_0\|_T)\right. \\
&\qquad \left. + s_1(v, v) + s_2(\boldsymbol{\sigma}, \boldsymbol{\sigma})\right).
\end{aligned}$$

Thus, using (3.1), (3.3), and the equation above we obtain

$$|\!|\!|v|\!|\!|_V^2 \le Ca(\boldsymbol{\sigma}, v; \boldsymbol{\sigma}, v). \tag{3.6}$$

Next, from (3.5), (3.1), and (3.6) we have

$$\begin{aligned}\sum_{T\in\mathcal{T}_h}\|\boldsymbol{\sigma}_0\|^2_{T,a^{-1}} &= \sum_{T\in\mathcal{T}_h}((\boldsymbol{\sigma}_0+a\nabla_w v,\ a^{-1}\boldsymbol{\sigma}_0)_T-(\nabla_w v,\ \boldsymbol{\sigma}_0)_T)\\ &= \sum_{T\in\mathcal{T}_h}((\boldsymbol{\sigma}_0+a\nabla_w v,\ \boldsymbol{\sigma}_0)_{T,a^{-1}}+(\nabla_w\cdot\boldsymbol{\sigma}+cv_0,\ v_0)_T-c(v_0,\ v_0)_T)\\ &+\sum_{T\in\mathcal{T}_h}\langle Q_b v_0-v_b,\ (\boldsymbol{\sigma}_0-\boldsymbol{\sigma}_b)\cdot\mathbf{n}\rangle_{\partial T}\\ &\le C\left(\sum_{T\in\mathcal{T}_h}(\|\boldsymbol{\sigma}_0+a\nabla_w v\|_{T,a^{-1}}\|\boldsymbol{\sigma}_0\|_{T,a^{-1}}+\|\nabla_w\cdot\boldsymbol{\sigma}+cv_0\|_T\|v_0\|_T)\right.\\ &\qquad\left.+s_1(v,v)+s_2(\boldsymbol{\sigma},\boldsymbol{\sigma})\right).\end{aligned}$$

Using the inequalities (3.1), (3.3), (3.4), and (3.6), we arrive at

$$\|\boldsymbol{\sigma}_0\|^2_{a^{-1}}\le Ca(\boldsymbol{\sigma},v;\boldsymbol{\sigma},v).$$

Similarly, we have from the Poincaré inequality (3.1) and the estimate (3.6) that

$$\|\nabla_w\cdot\boldsymbol{\sigma}\|^2\le C(\|\nabla_w\cdot\boldsymbol{\sigma}+cv_0\|^2+\|v_0\|^2)\le Ca(\boldsymbol{\sigma},v;\boldsymbol{\sigma},v).$$

Combining the two estimates above with (3.4) gives

$$|\!|\!|\boldsymbol{\sigma}|\!|\!|^2_\Sigma\le Ca(\boldsymbol{\sigma},v;\boldsymbol{\sigma},v),$$

which, together with (3.6), completes the proof of the lemma. ∎

LEMMA 3.2. *The weak Galerkin finite element scheme* (2.2) *has one and only one solution.*

Proof. It suffices to prove uniqueness. If $\mathbf{q}_h^{(1)}\times u_h^{(1)}$ and $\mathbf{q}_h^{(2)}\times u_h^{(2)}$ are two solutions of (2.2), then $\tau_h=u_h^{(1)}-u_h^{(2)}$ and $\boldsymbol{\eta}_h=\mathbf{q}_h^{(1)}-\mathbf{q}_h^{(2)}$ would satisfy the equation

$$a(\boldsymbol{\eta}_h,\tau_h;\boldsymbol{\sigma},v)=0\qquad\forall\boldsymbol{\sigma}\times v\in\Sigma_h\times V_h^0.$$

Note that $\tau_h\in V_h^0$. Then by letting $v=\tau_h$ and $\boldsymbol{\sigma}=\boldsymbol{\eta}_h$ in the above equation we arrive at

$$|\!|\!|\tau_h|\!|\!|^2_V+|\!|\!|\boldsymbol{\eta}_h|\!|\!|^2_\Sigma\le Ca_s(\boldsymbol{\eta}_h,\tau_h;\boldsymbol{\eta}_h,\tau_h)=0.$$

It follows that $\tau_h\equiv 0$ and $\boldsymbol{\eta}_h\equiv 0$ or, equivalently, $u_h^{(1)}\equiv u_h^{(2)}$ and $\mathbf{q}_h^{(1)}\equiv\mathbf{q}_h^{(2)}$. This completes the proof of the lemma. ∎

4. Error analysis. On each element $T\in\mathcal{T}_h$, denote by $\boldsymbol{\Pi}_h$ and Π_h the L^2 projections from $[L^2(T)]^d$ to $[P_k(T)]^d$ and from $L^2(T)$ to $P_k(T)$, respectively. Denote by Q_0 and Q_b the L^2 projections from $L^2(T)$ to $P_{k+1}(T)$ and from $L^2(e)$ to $P_k(e)$, respectively. Now define

$$Q_h u=\{Q_0u,Q_bu\}\in V_h,\quad \mathbf{Q}_h\mathbf{q}=\{\boldsymbol{\Pi}_h\mathbf{q},Q_b(\mathbf{q}\cdot\mathbf{n}_e)\mathbf{n}_e\}\in\Sigma_h.$$

LEMMA 4.1. *Let* $\alpha>\frac{1}{2}$. *Then, on each element* $T\in\mathcal{T}_h$, *we have the following operator identities:*

$$\boldsymbol{\Pi}_h\nabla v=\nabla_w(Q_hv),\qquad v\in H^1(T),\tag{4.1}$$

$$\Pi_h\nabla\cdot\boldsymbol{\sigma}=\nabla_w\cdot(\mathbf{Q}_h\boldsymbol{\sigma}),\qquad\boldsymbol{\sigma}\in[H^\alpha(T)]^d.\tag{4.2}$$

Proof. Using (2.4), integration by parts, and the definitions of Q_h and $\mathbf{\Pi}_h$, we have that for any $\tau \in [P_k(T)]^d$

$$\begin{aligned}(\nabla_w(Q_h v),\ \tau)_T &= -(Q_0 v,\ \nabla\cdot\tau)_T + \langle Q_b v,\ \tau\cdot\mathbf{n}\rangle_{\partial T}\\ &= -(v,\ \nabla\cdot\tau)_T + \langle v,\ \tau\cdot\mathbf{n}\rangle_{\partial T}\\ &= (\nabla v,\ \tau)_T = (\mathbf{\Pi}_h(\nabla v),\ \tau)_T,\end{aligned}$$

which implies the identity (4.1). Similarly we have that for any $\phi \in P_k(T)$

$$\begin{aligned}(\nabla_w\cdot(\mathbf{Q}_h\boldsymbol{\sigma}),\ \phi)_T &= -(\mathbf{\Pi}_h\boldsymbol{\sigma},\ \nabla\phi)_T + \langle Q_b(\boldsymbol{\sigma}\cdot\mathbf{n}_e)\mathbf{n}_e\cdot\mathbf{n},\ \phi\rangle_{\partial T}\\ &= -(\boldsymbol{\sigma},\ \nabla\phi)_T + \langle Q_b(\boldsymbol{\sigma}\cdot\mathbf{n}),\ \phi\rangle_{\partial T}\\ &= -(\boldsymbol{\sigma},\ \nabla\phi)_T + \langle\boldsymbol{\sigma}\cdot\mathbf{n},\ \phi\rangle_{\partial T}\\ &= (\nabla\cdot\boldsymbol{\sigma},\ \phi)_T = (\Pi_h(\nabla\cdot\boldsymbol{\sigma}),\ \phi)_T.\end{aligned}$$

This completes the proof of the lemma. ∎

Let $\mathbf{q}_h \times u_h \in \Sigma_h \times V_h$ be the weak Galerkin finite element solution arising from (2.2), and let $\mathbf{Q}_h\mathbf{q} \times Q_h u \in \Sigma_h \times V_h$ be the L^2 projection of the exact solution $\mathbf{q} \times u$. Their differences are referred to as the error functions, and they are denoted by

$$\boldsymbol{\varepsilon}_h = \mathbf{Q}_h\mathbf{q} - \mathbf{q}_h, \quad e_h = Q_h u - u_h. \tag{4.3}$$

For any given $\mathbf{q}$ and u, we introduce two linear forms on $\Sigma_h \times V_h$ as follows:

$$\begin{aligned}\ell_1(\mathbf{q}, u; \boldsymbol{\sigma}, v) &= \sum_{T\in\mathcal{T}_h} ((\mathbf{\Pi}_h - I)\mathbf{q} + a(\mathbf{\Pi}_h - I)\nabla u,\ \boldsymbol{\sigma}_0 + a\nabla_w v)_{T,a^{-1}},\\ \ell_2(\mathbf{q}, u; \boldsymbol{\sigma}, v) &= \sum_{T\in\mathcal{T}_h} ((\Pi_h - I)\nabla\cdot\mathbf{q} + c(\Pi_h - I)u,\ \nabla_w\cdot\boldsymbol{\sigma} + cv_0)_T.\end{aligned}$$

LEMMA 4.2. *Let $\mathbf{q} \times u$ be the exact solution of (1.3)–(1.5), and let $\mathbf{q}_h \times u_h \in \Sigma_h \times V_h$ be the weak Galerkin finite element solution arising from (2.2). The error function $\boldsymbol{\varepsilon}_h \times e_h$ satisfies the equations*

$$a(\boldsymbol{\varepsilon}_h, e_h; \boldsymbol{\sigma}, v) = \ell_{\mathbf{q},u}(\boldsymbol{\sigma}, v) \qquad \forall \boldsymbol{\sigma} \times v \in \Sigma_h \times V_h^0, \tag{4.4}$$

where

$$\ell_{\mathbf{q},u}(\boldsymbol{\sigma}, v) := \ell_1(\mathbf{q}, u; \boldsymbol{\sigma}, v) + \ell_2(\mathbf{q}, u; \boldsymbol{\sigma}, v) + s_1(Q_h u, v) + s_2(\mathbf{Q}_h\mathbf{q}, \boldsymbol{\sigma}). \tag{4.5}$$

Proof. From (4.1) and the fact that $\mathbf{q} + a\nabla u = 0$ we obtain

$$\mathbf{\Pi}_h\mathbf{q} + a\nabla_w Q_h u = \mathbf{\Pi}_h\mathbf{q} - \mathbf{q} - a(\nabla u - \mathbf{\Pi}_h\nabla u).$$

Hence, for any $\boldsymbol{\sigma} \times v \in \Sigma_h \times V_h^0$ we have

$$\begin{aligned}&\sum_{T\in\mathcal{T}_h} (\mathbf{\Pi}_h\mathbf{q} + a\nabla_w Q_h u,\ \boldsymbol{\sigma}_0 + a\nabla_w v)_{T,a^{-1}}\\ &= \sum_{T\in\mathcal{T}_h} (\mathbf{\Pi}_h\mathbf{q} - \mathbf{q} - a(\nabla u - \mathbf{\Pi}_h\nabla u),\ \boldsymbol{\sigma}_0 + a\nabla_w v)_{T,a^{-1}}\\ &= \ell_1(\mathbf{q}, u; \boldsymbol{\sigma}, v).\end{aligned} \tag{4.6}$$

Next, from (4.2) and the equation $\nabla \cdot \mathbf{q} + cu = f$ we have

$$\begin{aligned}\nabla_w \cdot \mathbf{Q}_h\mathbf{q} + c\Pi_h u &= \Pi_h \nabla \cdot \mathbf{q} + c\Pi_h u \\ &= f + (\Pi_h - I)\nabla \cdot \mathbf{q} + c(\Pi_h - I)u.\end{aligned}$$

Thus, testing the above against $\nabla_w \cdot \boldsymbol{\sigma} + cv_0$ on each element gives rise to

$$\begin{aligned}&\sum_{T\in\mathcal{T}_h} (\nabla_w \cdot \mathbf{Q}_h\mathbf{q} + c\Pi_h u,\ \nabla_w \cdot \boldsymbol{\sigma} + cv_0)_T \\ &= (f,\ \nabla_w \cdot \boldsymbol{\sigma} + cv_0) + \ell_2(\mathbf{q}, u; \boldsymbol{\sigma}, v).\end{aligned} \tag{4.7}$$

Summing (4.6) with (4.7) yields

$$\begin{aligned}\sum_{T\in\mathcal{T}_h} ((\boldsymbol{\Pi}_h\mathbf{q} + a\nabla_w Q_h u,\ \boldsymbol{\sigma}_0 + a\nabla_w v)_{T,a^{-1}} + (\nabla_w \cdot \mathbf{Q}_h\mathbf{q} + c\Pi_h u,\ \nabla_w \cdot \boldsymbol{\sigma} + cv_0)_T) \\ = (f,\ \nabla_w \cdot \boldsymbol{\sigma} + cv_0) + \ell_1(\mathbf{q}, u; \boldsymbol{\sigma}, v) + \ell_2(\mathbf{q}, u; \boldsymbol{\sigma}, v).\end{aligned}$$

Adding $s_1(Q_h u, v)$ and $s_2(\mathbf{Q}_h\mathbf{q}, \boldsymbol{\sigma})$ to both sides of the above equation, we obtain

$$\begin{aligned}a(\mathbf{Q}_h\mathbf{q}, Q_h u; \boldsymbol{\sigma}, v) &= (f, \nabla_w \cdot \boldsymbol{\sigma} + cv_0) + \ell_1(\mathbf{q}, u; \boldsymbol{\sigma}, v) \\ &\quad + \ell_2(\mathbf{q}, u; \boldsymbol{\sigma}, v) + s_1(Q_h u, v) + s_2(\mathbf{Q}_h\mathbf{q}, \boldsymbol{\sigma}).\end{aligned} \tag{4.8}$$

The difference between (4.8) and (2.2) yields the error equation (4.4). ∎

Remark 4.3. If the coefficients a and c in (1.1) are constants on each element $T \in \mathcal{T}_h$, then the usual L^2 orthogonality of the projection operator Π_h and $\boldsymbol{\Pi}_h$ implies

$$\begin{aligned}((\boldsymbol{\Pi}_h - I)\mathbf{q} + a(\boldsymbol{\Pi}_h - I)\nabla u,\ \boldsymbol{\sigma}_0 + a\nabla_w v)_{T,a^{-1}} = 0, \\ ((\Pi_h - I)\nabla \cdot \mathbf{q} + c(\Pi_h - I)u,\ \nabla_w \cdot \boldsymbol{\sigma} + cv_0)_T = 0.\end{aligned}$$

Thus, we have $\ell_1 \equiv 0$ and $\ell_2 \equiv 0$. Consequently, the linear form $\ell_{\mathbf{q},u}$ in (4.4) takes the following simplified form:

$$\ell_{\mathbf{q},u}(\boldsymbol{\sigma}, v) = s_1(Q_h u, v) + s_2(\mathbf{Q}_h\mathbf{q}, \boldsymbol{\sigma}). \tag{4.9}$$

We now turn our attention to some technical inequalities that will be used to estimate the linear functional $\ell_{\mathbf{q},u}$ in (4.4). To this end, let T be an element with e as an edge. For any function $\varphi \in H^1(T)$, the following trace inequality holds true (see [37] for details):

$$\|\varphi\|_e^2 \le C\left(h_T^{-1}\|\varphi\|_T^2 + h_T\|\nabla\varphi\|_T^2\right). \tag{4.10}$$

Using the trace inequality (4.10) we can establish the following result.

LEMMA 4.4. *Assume that $\mathcal{T}_h$ is shape-regular, and the coefficient c is C^1 on each element T. Then for $u \in H^{k+2}(\Omega)$ and $\mathbf{q} \in [H^{k+1}(\Omega)]^d$, we have*

$$|s_1(Q_h u, v)| \le Ch^{k+1}\|u\|_{k+2}|\!|\!|v|\!|\!|_V, \tag{4.11}$$

$$|s_2(\mathbf{Q}_h\mathbf{q}, \boldsymbol{\sigma})| \le Ch^{k+1}\|\mathbf{q}\|_{k+1}|\!|\!|\boldsymbol{\sigma}|\!|\!|_\Sigma, \tag{4.12}$$

$$|\ell_1(\mathbf{q}, u; \boldsymbol{\sigma}, v)| \le Ch^{k+1}(\|\mathbf{q}\|_{k+1} + \|u\|_{k+2})(|\!|\!|\boldsymbol{\sigma}|\!|\!|_\Sigma + |\!|\!|v|\!|\!|_V), \tag{4.13}$$

$$|\ell_2(\mathbf{q}, u; \boldsymbol{\sigma}, v)| \le Ch^{k+1}(\|\nabla \cdot \mathbf{q}\|_k + \|u\|_{k+1})(|\!|\!|\boldsymbol{\sigma}|\!|\!|_\Sigma + |\!|\!|v|\!|\!|_V). \tag{4.14}$$

Proof. Using the definition of Q_b and the trace inequality (4.10), we obtain

$$\begin{aligned}
|s_1(Q_h u, v)| &= \left| \sum_{T\in\mathcal{T}_h} h^{-1}\langle Q_b(Q_0 u) - Q_b u,\ Q_b v_0 - v_b\rangle_{\partial T} \right| \\
&= \left| \sum_{T\in\mathcal{T}_h} h^{-1}\langle Q_0 u - u,\ Q_b v_0 - v_b\rangle_{\partial T} \right| \\
&\le C \left(\sum_{T\in\mathcal{T}_h} (h^{-2}\|Q_0 u - u\|_T^2 + \|\nabla(Q_0 u - u)\|_T^2) \right)^{\frac{1}{2}} \\
&\quad \cdot \left(\sum_{T\in\mathcal{T}_h} h^{-1}\|Q_b v_0 - v_b\|_{\partial T}^2 \right)^{\frac{1}{2}} \\
&\le C h^{k+1}\|u\|_{k+2}|\!|\!|v|\!|\!|_V.
\end{aligned}$$

Similarly, we have

$$\begin{aligned}
|s_2(\mathbf{Q}_h\mathbf{q}, \boldsymbol{\sigma})| &= \left| \sum_{T\in\mathcal{T}_h} h\langle \boldsymbol{\Pi}_h\mathbf{q}\cdot\mathbf{n} - Q_b(\mathbf{q}\cdot\mathbf{n}_e)\mathbf{n}_e\cdot\mathbf{n},\ (\boldsymbol{\sigma}_0 - \boldsymbol{\sigma}_b)\cdot\mathbf{n}\rangle_{\partial T} \right| \\
&= \left| \sum_{T\in\mathcal{T}_h} h\langle \boldsymbol{\Pi}_h\mathbf{q}\cdot\mathbf{n} - Q_b(\mathbf{q}\cdot\mathbf{n}),\ (\boldsymbol{\sigma}_0 - \boldsymbol{\sigma}_b)\cdot\mathbf{n}\rangle_{\partial T} \right| \\
&= \left| \sum_{T\in\mathcal{T}_h} h\langle \boldsymbol{\Pi}_h\mathbf{q}\cdot\mathbf{n} - \mathbf{q}\cdot\mathbf{n},\ (\boldsymbol{\sigma}_0 - \boldsymbol{\sigma}_b)\cdot\mathbf{n}\rangle_{\partial T} \right| \\
&\le C h^{k+1}\|\mathbf{q}\|_{k+1}|\!|\!|\boldsymbol{\sigma}|\!|\!|_\Sigma.
\end{aligned}$$

To derive (4.13), we use the standard error estimate for L^2 projections to obtain

$$\begin{aligned}
|\ell_1(\mathbf{q}, u; \boldsymbol{\sigma}, v)| &= \left| \sum_{T\in\mathcal{T}_h} (\mathbf{q} - \boldsymbol{\Pi}_h\mathbf{q} + a(\nabla u - \boldsymbol{\Pi}_h\nabla u),\ \boldsymbol{\sigma}_0 + a\nabla_w v)_{T,a^{-1}} \right| \\
&\le C \sum_{T\in\mathcal{T}_h} (\|\mathbf{q} - \boldsymbol{\Pi}_h\mathbf{q}\|_{T,a^{-1}} + \|\nabla u - \boldsymbol{\Pi}_h\nabla u\|_{T,a})\|\boldsymbol{\sigma}_0 + a\nabla_w v\|_{T,a^{-1}} \\
&\le C h^{k+1}(\|\mathbf{q}\|_{k+1} + \|u\|_{k+2})(|\!|\!|\boldsymbol{\sigma}|\!|\!|_\Sigma + |\!|\!|v|\!|\!|_V).
\end{aligned}$$

To derive (4.14), let $\bar{c}$ be the average of c on each element T. The L^2 orthogonality of the projection operator Π_h implies

$$\begin{aligned}
&((\Pi_h - I)\nabla\cdot\mathbf{q} + c(\Pi_h - I)u,\ \nabla_w\cdot\boldsymbol{\sigma} + cv_0)_T \\
&= ((\Pi_h - I)\nabla\cdot\mathbf{q}, (c - \bar{c})v_0)_T + (c(\Pi_h - I)u,\ \nabla_w\cdot\boldsymbol{\sigma} + cv_0)_T.
\end{aligned}$$

Hence,

$$\begin{aligned}
&|((\Pi_h - I)\nabla\cdot\mathbf{q} + c(\Pi_h - I)u,\ \nabla_w\cdot\boldsymbol{\sigma} + cv_0)_T| \\
&\le \|(\Pi_h - I)\nabla\cdot\mathbf{q}\|_T\|(c - \bar{c})v_0\|_T + \|c(\Pi_h - I)u\|_T\|\nabla_w\cdot\boldsymbol{\sigma} + cv_0\|_T \\
&\le C h^{k+1}\|\nabla\cdot\mathbf{q}\|_{k,T}\|v_0\|_T + C h^{k+1}\|u\|_{k+1,T}\|\ \|\nabla_w\cdot\boldsymbol{\sigma} + cv_0\|_T.
\end{aligned}$$

It follows that

$$\begin{aligned}|\ell_2(\mathbf{q},u;\boldsymbol{\sigma},v)| &= \left|\sum_{T\in\mathcal{T}_h}((\Pi_h-I)\nabla\cdot\mathbf{q}+c(\Pi_h-I)u,\ \nabla_w\cdot\boldsymbol{\sigma}+cv_0)_T\right|\\ &\le \sum_{T\in\mathcal{T}_h}|((\Pi_h-I)\nabla\cdot\mathbf{q}+c(\Pi_h-I)u,\ \nabla_w\cdot\boldsymbol{\sigma}+cv_0)_T|\\ &\le Ch^{k+1}\sum_{T\in\mathcal{T}_h}(\|\nabla\cdot\mathbf{q}\|_{k,T}\|v_0\|_T+\|u\|_{k+1,T}\|\ \|\nabla_w\cdot\boldsymbol{\sigma}+cv_0\|_T)\\ &\le Ch^{k+1}(\|\nabla\cdot\mathbf{q}\|_k+\|u\|_{k+1})(|\!|\!|\boldsymbol{\sigma}|\!|\!|_\Sigma+|\!|\!|v|\!|\!|_V).\end{aligned}$$

This completes the proof of the lemma. ∎

THEOREM 4.5. *Let $\mathbf{q}_h\times u_h\in\Sigma_h\times V_h$ be the weak Galerkin least-squares finite element solution of the problem (1.3)–(1.5) arising from (2.2). Assume the exact solution $u\in H^{k+2}(\Omega)$ and $\mathbf{q}\in[H^{k+1}(\Omega)]^d$. Under the assumptions of Lemma 4.4, there exists a constant C such that*

$$|\!|\!|u_h-Q_hu|\!|\!|_V+|\!|\!|\mathbf{q}_h-\mathbf{Q}_h\mathbf{q}|\!|\!|_\Sigma\le Ch^{k+1}(\|u\|_{k+2}+\|\mathbf{q}\|_{k+1}). \tag{4.15}$$

Proof. By letting $v=e_h$ and $\boldsymbol{\sigma}=\boldsymbol{\varepsilon}_h$ in (4.4), we have

$$a(\boldsymbol{\varepsilon}_h,e_h;\boldsymbol{\varepsilon}_h,e_h)=\ell_{\mathbf{q},u}(\boldsymbol{\varepsilon}_h,e_h), \tag{4.16}$$

where

$$\ell_{\mathbf{q},u}(\boldsymbol{\varepsilon}_h,e_h)=\ell_1(\mathbf{q},u;\boldsymbol{\varepsilon}_h,e_h)+\ell_2(\mathbf{q},u;\boldsymbol{\varepsilon}_h,e_h)+s_1(Q_hu,e_h)+s_2(\mathbf{Q}_h\mathbf{q},\boldsymbol{\varepsilon}_h).$$

It then follows from (3.2) and the estimates (4.11)–(4.14) that

$$|\!|\!|e_h|\!|\!|_V+|\!|\!|\boldsymbol{\varepsilon}_h|\!|\!|_\Sigma\le Ch^{k+1}(\|u\|_{k+2}+\|\mathbf{q}\|_{k+1}),$$

which implies (4.15). This completes the proof. ∎

5. A Schur complement formulation. In this section we develop a Schur complement formulation for the weak Galerkin scheme (2.2) by eliminating all the unknowns corresponding to $\mathbf{q}_0$ and u_0 from the linear system arising from the scheme (2.2).

Let $\mathbf{q}_h\times u_h\in\Sigma_h\times V_h$ be the solution of (2.2). By restricting test functions as $\boldsymbol{\sigma}\times v=\{\boldsymbol{\sigma}_0,0\}\times\{v_0,0\}$ we arrive at the following equation:

$$a(\mathbf{q}_h,u_h;\boldsymbol{\sigma},v)=(f,\ \nabla_w\cdot\boldsymbol{\sigma}+cv_0)\quad\forall\{\boldsymbol{\sigma}_0,0\}\times\{v_0,0\}\in\Sigma_h\times V_h^0. \tag{5.1}$$

Next, by taking the test function $\boldsymbol{\sigma}\times v$ as $\{0,\boldsymbol{\sigma}_b\}\times\{0,v_b\}$ we have

$$a(\mathbf{q}_h,u_h;\boldsymbol{\sigma},v)=(f,\ \nabla_w\cdot\boldsymbol{\sigma})\quad\forall\{0,\boldsymbol{\sigma}_b\}\times\{0,v_b\}\in\Sigma_h\times V_h^0. \tag{5.2}$$

Hence, the weak Galerkin finite element scheme (2.2) is equivalent to the following scheme: *Find $\mathbf{q}_h\times u_h\in\Sigma_h\times V_h$ satisfying* (1) $u_b=Q_bg$ *on* $\partial\Omega$, *and* (2) *the system of linear equations* (5.1) *and* (5.2).

Note that if u_b, $\mathbf{q}_b$ and f are given, then u_0 and $\mathbf{q}_0$ are determined locally by the system of linear equations (5.1) on each element T. We denote this dependence as

$$u_0=u_0(u_b,\mathbf{q}_b,f),\qquad \mathbf{q}_0=\mathbf{q}_0(u_b,\mathbf{q}_b,f)$$

and further write

$$u_h = u_h(u_b, \mathbf{q}_b, f) = \{u_0(u_b, \mathbf{q}_b, f), u_b\} \in V_h, \tag{5.3}$$

$$\mathbf{q}_h = \mathbf{q}_h(u_b, \mathbf{q}_b, f) = \{\mathbf{q}_0(u_b, \mathbf{q}_b, f), \mathbf{q}_b\} \in \Sigma_h. \tag{5.4}$$

The principle of superposition then implies

$$u_h(u_b, \mathbf{q}_b, f) = u_h(u_b, \mathbf{q}_b, 0) + u_h(0, 0, f), \tag{5.5}$$

$$\mathbf{q}_h(u_b, \mathbf{q}_b, f) = \mathbf{q}_h(u_b, \mathbf{q}_b, 0) + \mathbf{q}_h(0, 0, f). \tag{5.6}$$

By substituting (5.5) and (5.6) into (5.2), we have

$$a(\mathbf{q}_h(u_b, \mathbf{q}_b, 0), u_h(u_b, \mathbf{q}_b, 0); \boldsymbol{\sigma}, v) = (f, \nabla_w \cdot \boldsymbol{\sigma}) - a(\mathbf{q}_h(0, 0, f), u_h(0, 0, f); \boldsymbol{\sigma}, v) \tag{5.7}$$

for all $v = \{0, v_b\} \in V_h^0$ and $\boldsymbol{\sigma} = \{0, \boldsymbol{\sigma}_b\} \in \Sigma_h$. The system of linear equations (5.7) is the Schur complement of the weak Galerkin finite element scheme (2.2) through local eliminations of $\mathbf{q}_0$ and u_0.

LEMMA 5.1. *The matrix corresponding to the system of linear equations* (5.7) *is symmetric and positive definite.*

Proof. From the definition of $u_h(u_b, \mathbf{q}_b, 0)$, $\mathbf{q}_h(u_b, \mathbf{q}_b, 0)$, and (5.1) we have

$$a(\mathbf{q}_h(u_b, \mathbf{q}_b, 0), u_h(u_b, \mathbf{q}_b, 0); \boldsymbol{\sigma}, v) = 0 \tag{5.8}$$

for all $v = \{v_0, 0\} \in V_h^0$ and $\boldsymbol{\sigma} = \{\boldsymbol{\sigma}_0, 0\} \in \Sigma_h$. Combining (5.3)–(5.4) with $f = 0$ and (5.8) gives

$$\begin{aligned} &a(\mathbf{q}_h(u_b, \mathbf{q}_b, 0), u_h(u_b, \mathbf{q}_b, 0); \boldsymbol{\sigma}, v) \\ &= a(\mathbf{q}_h(u_b, \mathbf{q}_b, 0), u_h(u_b, \mathbf{q}_b, 0); \boldsymbol{\sigma}(v_b, \boldsymbol{\sigma}_b, 0), v(v_b, \boldsymbol{\sigma}_b, 0)) \end{aligned}$$

for all $v = \{0, v_b\} \in V_h^0$ and $\boldsymbol{\sigma} = \{0, \boldsymbol{\sigma}_b\} \in \Sigma_h$. It follows that the system (5.7) is symmetric.

Next we show that $v_b = 0$ and $\boldsymbol{\sigma}_b = 0$ for $v = \{0, v_b\} \in V_h^0$ and $\boldsymbol{\sigma} = \{0, \boldsymbol{\sigma}_b\} \in \Sigma_h$ if

$$a(\boldsymbol{\sigma}(v_b, \boldsymbol{\sigma}_b, 0), v(v_b, \boldsymbol{\sigma}_b, 0); \boldsymbol{\sigma}(v_b, \boldsymbol{\sigma}_b, 0), v(v_b, \boldsymbol{\sigma}_b, 0)) = 0. \tag{5.9}$$

If fact, from (5.9) and the coercivity estimate (3.2) we clearly have $v(v_b, \boldsymbol{\sigma}_b, 0) = 0$ and $\boldsymbol{\sigma}(v_b, \boldsymbol{\sigma}_b, 0) = 0$, which implies $v_b = 0$ and $\boldsymbol{\sigma}_b = 0$. This completes the proof of the lemma. ∎

It should be pointed out that the Schur complement (5.7) is a version of the weak Galerkin least-squares finite element scheme (2.2) that involves fewer unknowns than the original formulation. In fact, the only unknown variables that enter into the Schur complement are those corresponding to u_b and $\mathbf{q}_b$ defined on the boundary of each element. Due to this significant size reduction, the Schur complement can be regarded as an efficient implementation of the weak Galerkin least-squares finite element scheme (2.2).

6. Numerical experiments. In this section, we shall conduct several numerical experiments by using the weak Galerkin finite element method proposed in section 2. The first five numerical examples will make use of the lowest order weak Galerkin element; i.e., $u_0 \in P_1(T)$, $u_b \in P_0(e)$, $\boldsymbol{\sigma}_0 \in [P_0(T)]^2$, $\boldsymbol{\sigma}_b|_e = \sigma_b \mathbf{n}_e$ with $\sigma_b \in P_0(e)$.

TABLE 6.1
Example 1: *The rates of convergence in the discrete H^1- and L^2-norms on triangular meshes.*

c	h	H^1-error	Order	L^2-error	Order
0	1/4	1.2784e-02		6.9336e-04	
	1/8	6.3731e-03	1.0043	1.8695e-04	1.8910
	1/16	3.1842e-03	1.0011	4.7889e-05	1.9649
	1/32	1.5918e-03	1.0003	1.2062e-05	1.9892
	1/64	7.9588e-04	1.0000	3.0221e-06	1.9968
	1/128	3.9794e-04	1.0000	7.5600e-07	1.9991
10	1/4	3.6631e-02		3.9172e-03	
	1/8	1.0761e-02	1.7673	6.2029e-04	2.6588
	1/16	3.8547e-03	1.4811	1.2186e-04	2.3477
	1/32	1.6820e-03	1.1964	2.8000e-05	2.1217
	1/64	8.0739e-04	1.0588	6.8374e-06	2.0339
	1/128	3.9938e-04	1.0155	1.6991e-06	2.0087
−10	1/4	1.8697e-02		2.7990e-03	
	1/8	7.3110e-03	1.3547	8.1322e-04	1.7832
	1/16	3.3110e-03	1.1428	2.1422e-04	1.9246
	1/32	1.6080e-03	1.0420	5.4318e-05	1.9796
	1/64	7.9791e-04	1.0110	1.3629e-05	1.9948
	1/128	3.9819e-04	1.0028	3.4104e-06	1.9987

Let $u_h = \{u_0, u_b\}$ and $\mathbf{q}_h$ be the solutions to the weak Galerkin equation (2.2), and let $\mathbf{q} \times u$ be the exact solution of the original equation (1.3)–(1.5). The errors are given by $\boldsymbol{\varepsilon}_h = \mathbf{Q}_h\mathbf{q} - \mathbf{q}_h$ and $e_h = Q_h u - u_h$, where $\mathbf{Q}_h$ and Q_h are the L^2 projections of $\mathbf{q}$ and u onto the corresponding weak Galerkin finite element spaces. The following norms are used in the numerical tests:

$$H^1\text{-norm: } \sqrt{|||v|||_V^2 + |||\boldsymbol{\sigma}|||_\Sigma^2} = \sqrt{a(\boldsymbol{\sigma}, v; \boldsymbol{\sigma}, v)}, \tag{6.1}$$

$$L^2\text{-norm: } \|u_0 - Q_0 u\| = \left(\sum_{T \in \mathcal{T}_h} \int_T |u_0 - Q_0 u|^2 dx \right)^{1/2}, \tag{6.2}$$

$$L^1\text{-norm: } \|u_0 - Q_0 u\|_{L^1} = \sum_{T \in \mathcal{T}_h} \int_T |u_0 - Q_0 u| dx, \tag{6.3}$$

$$W^{1,1}\text{-seminorm: } |u_0 - Q_0 u|_{1,1} = \sum_{T \in \mathcal{T}_h} \int_T |\nabla(u_0 - Q_0 u)| dx. \tag{6.4}$$

6.1. Example 1. Consider the second order elliptic equation (1.1) with Dirichlet boundary condition on the uniform triangular meshes for $\Omega = (0,1) \times (0,1)$. We use a test problem with exact solution

$$u = -\left(\frac{x^2}{2} - \frac{x^3}{3}\right)\left(\frac{y^2}{2} - \frac{y^3}{3}\right).$$

The coefficient a is fixed as $a = 1$ and various values of the coefficient c are tested in our numerical experiments. The right-hand side function f and the boundary value are determined from (1.1)–(1.2) and the selected values for a and c.

The numerical results for the cases $c = 0$ and $c = 10$ are reported in Table 6.1. The theoretical error estimate asserts the first and second order of convergence in the H^1- and L^2-norms, respectively. This theory is confirmed by the numerical results in Table 6.1. We also tested the numerical algorithm (2.2) with the negative value

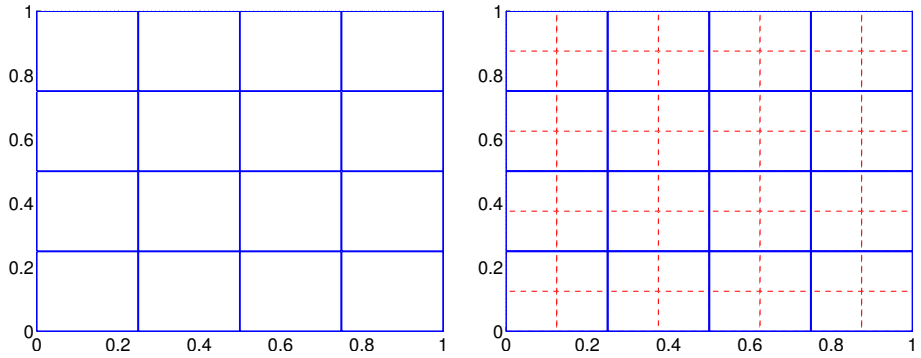

FIG. 6.1. *Example* 2: *Mesh level* 1 *for* $n = 4$ *(left); mesh level* 2 *for* $n = 8$ *(right).*

TABLE 6.2
Example 2: *The rates of convergence in the discrete* H^1*- and* L^2*-norms for uniform rectangular partitions.*

c	h	H^1-error	Order	L^2-error	Order
0	1/4	4.1980e-02		4.0075e-03	
	1/8	1.4791e-02	1.5050	1.0424e-03	1.9428
	1/16	6.1894e-03	1.2568	2.6718e-04	1.9640
	1/32	2.9157e-03	1.0860	6.7327e-05	1.9886
	1/64	1.4343e-03	1.0235	1.6867e-05	1.9770
	1/128	7.1418e-04	1.0060	4.2190e-06	1.9992
10	1/4	5.4470e-02		1.1937e-03	
	1/8	1.6937e-02	1.6853	2.2250e-04	2.4236
	1/16	6.5055e-03	1.3804	7.3914e-05	1.5899
	1/32	2.9576e-03	1.1372	2.0209e-05	1.8708
	1/64	1.4396e-03	1.0388	5.1687e-06	1.9671
	1/128	7.1485e-04	1.0100	1.2996e-06	1.9917
−10	1/4	6.3193e-02		2.5404e-02	
	1/8	2.0838e-02	1.6005	8.6091e-03	1.5611
	1/16	7.3299e-03	1.5074	2.3777e-03	1.8563
	1/32	3.0823e-03	1.2498	6.1070e-04	1.9610
	1/64	1.4561e-03	1.0819	1.5373e-04	1.9901
	1/128	7.1694e-04	1.0222	3.8500e-05	1.9975

of $c = -10$. Table 6.1 shows the corresponding numerical results which illustrate an optimal rate of convergence in the usual H^1- and L^2-norms.

6.2. Example 2. In this example, we shall test the performance of the weak Galerkin least-squares algorithm on uniform rectangular partitions. The domain is fixed as $\Omega = (0,1) \times (0,1)$ and the function f in (1.1) is chosen so that the exact solution is given by

$$u = x(1-x)y(1-y).$$

The rectangular partitions are constructed by partitioning the domain into $n \times n$ uniform subrectangles so that the mesh size is given by $h = 1/n$. The rectangular partitions with $n = 4$ and $n = 8$ are plotted in Figure 6.1.

The weak Galerkin algorithm (2.2) is tested for $a = 1$ and various values of c. The numerical results for $c = 0$, $c = 10$, and $c = -10$ are illustrated in Table 6.2. Optimal rates of convergence are observed when measured in the discrete H^1- and L^2-norms, which are consistent with the convergence theory. Again, we detected the convergence rates of $O(h)$ and $O(h^2)$ in the discrete H^1- and L^2-norms for the case $c = -10$.

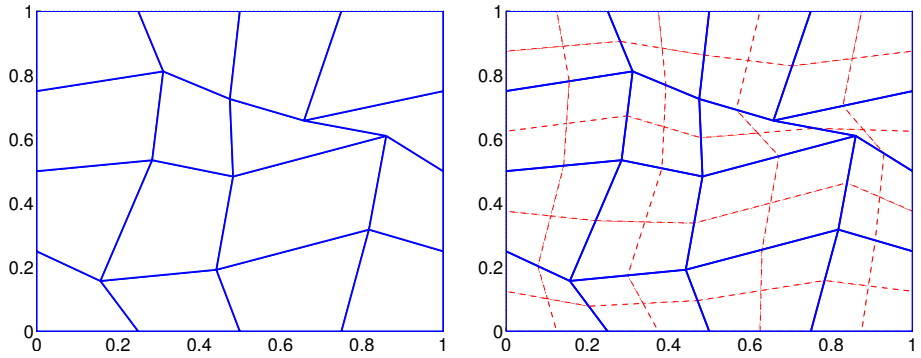

FIG. 6.2. *Example* 3: *Mesh level* 1 *(left); mesh level* 2 *(right).*

TABLE 6.3
Example 3: *The rates of convergence in the discrete* H^1*- and* L^2*-norms on deformed meshes.*

c	h	L^2-error	Order	L^2-error	Order
0	3.2327e-01	6.1187e-02		5.4044e-03	
	1.6178e-01	2.1245e-02	1.5281	1.5135e-03	1.8386
	8.0929e-02	8.4355e-03	1.3335	4.0547e-04	1.9015
	4.0847e-02	3.8201e-03	1.1586	1.0480e-04	1.9788
	2.0610e-02	1.8519e-03	1.0585	2.6515e-05	2.0091
	1.0351e-02	9.1819e-04	1.0187	6.6586e-06	2.0064
10	3.2327e-01	7.5076e-02		1.7556e-03	
	1.6178e-01	2.3652e-02	1.6685	4.0390e-04	2.1226
	8.0929e-02	8.7989e-03	1.4276	1.2261e-04	1.7211
	4.0847e-02	3.8691e-03	1.2016	3.3632e-05	1.8918
	2.0610e-02	1.8582e-03	1.0722	8.6862e-06	1.9790
	1.0351e-02	9.1897e-04	1.0224	2.1969e-06	1.9961
−10	3.2327e-01	8.1395e-02		2.8274e-02	
	1.6178e-01	2.8009e-02	1.5410	1.0589e-02	1.4187
	8.0929e-02	9.8771e-03	1.5048	3.1113e-03	1.7682
	4.0847e-02	4.0470e-03	1.3049	8.1955e-04	1.9511
	2.0610e-02	1.8825e-03	1.1189	2.0793e-04	2.0050
	1.0351e-02	9.2209e-04	1.0363	5.2196e-05	2.0070

6.3. Example 3. The goal of this test case is to examine the performance of the weak Galerkin least-square finite element method on deformed rectangular meshes. The unit square domain is used in this numerical experiment, and the initial deformed mesh is shown in Figure 6.2 (left). The initial partition is then refined successively by connecting the barycenter of each element with the midpoint of each edge in the same element, as shown in Figure 6.2 (right).

The test problem is the same as in Example 2. The difference between Examples 2 and 3 is between the finite element partitions: one is a uniform partition with rectangles, and the other is made of deformed rectangles with hanging nodes. In the weak Galerkin algorithm, no nodes are actually hanging, as the triangle with a "hanging" node on one of its edges was treated as a deformed rectangle or a degenerate quadrilateral. The corresponding numerical results are shown in Table 6.3, which are consistent with the error estimates established in the previous sections.

6.4. Example 4. The test problem is given by a differential equation arising from the modeling of fluid flow in porous media with strong anisotropic permeability.

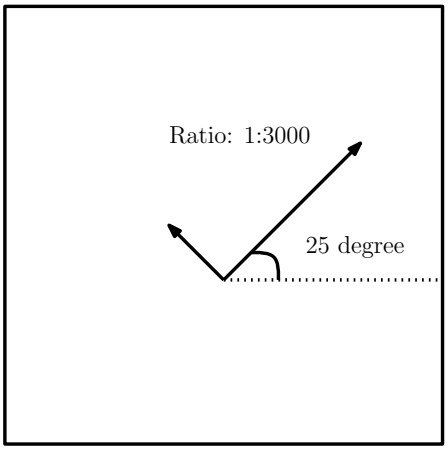

FIG. 6.3. *Example* 4: *A strong anisotropic permeability.*

The model problem seeks an unknown pressure function $u = u(x)$ such that

$$\begin{aligned} -\nabla \cdot (a\nabla u) &= f \quad \text{in } \Omega, \\ u &= g \quad \text{on } \partial\Omega. \end{aligned}$$

The domain is the unit square $\Omega = (0,1)^2$, and the permeability tensor is given by

$$a = \begin{pmatrix} 0.246436002 & 0.114868364 \\ 0.114868364 & 0.053663998 \end{pmatrix}. \tag{6.5}$$

This test problem is chosen from [24] (see Example 2).

Note that the anisotropy for this test problem is $1:3000$, which is the ratio of the two positive eigenvalues of the 2×2 permeability tensor, as shown in Figure 6.3. The exact solution for this test problem is chosen as

$$u(x,y) = \exp\left(-\frac{(x-x_c)^2 + (y-y_c)^2}{2\sigma^2}\right),$$

where $(x_c, y_c) = (0.5, 0.5)$ and $\sigma^2 = 0.005$. The source term f can be calculated as

$$f(x,y) = f^*(x,y)\exp\left(-\frac{(x-x_c)^2 + (y-y_c)^2}{2\sigma^2}\right),$$

with

$$f^*(x,y) = \left(\frac{1}{\sigma^2}(a^* + d^*) - \frac{1}{\sigma^4}(a^*(x-x_c)^2 + 2b^*(x-x_c)(y-y_c) + d^*(y-y_c)^2)\right),$$

where $a^* = 0.246436002,\ b^* = 0.114868364$, and $d^* = 0.053663998$.

Our numerical results are based on the finite element scheme (2.2) with the lowest order elements (i.e., $u_0 \in P_1(T),\ u_b \in P_0(e),\ \boldsymbol{\sigma}_0 \in [P_0(T)]^2,\ \boldsymbol{\sigma}_b|_e = \sigma_b \mathbf{n}_e$ with $\sigma_b \in P_0(e)$) on the uniform triangular meshes. Contour plots for the numerical solution u_h for mesh sizes $h = 1/32,\ h = 1/48,\ h = 1/64,\ h = 1/96$ are shown in Figure 6.4. As $\boldsymbol{\sigma}$ assumes a small value, the pressure u is concentrated at the point $(0.5, 0.5)$. The contour plots indicate that the solution of the weak Galerkin algorithm has

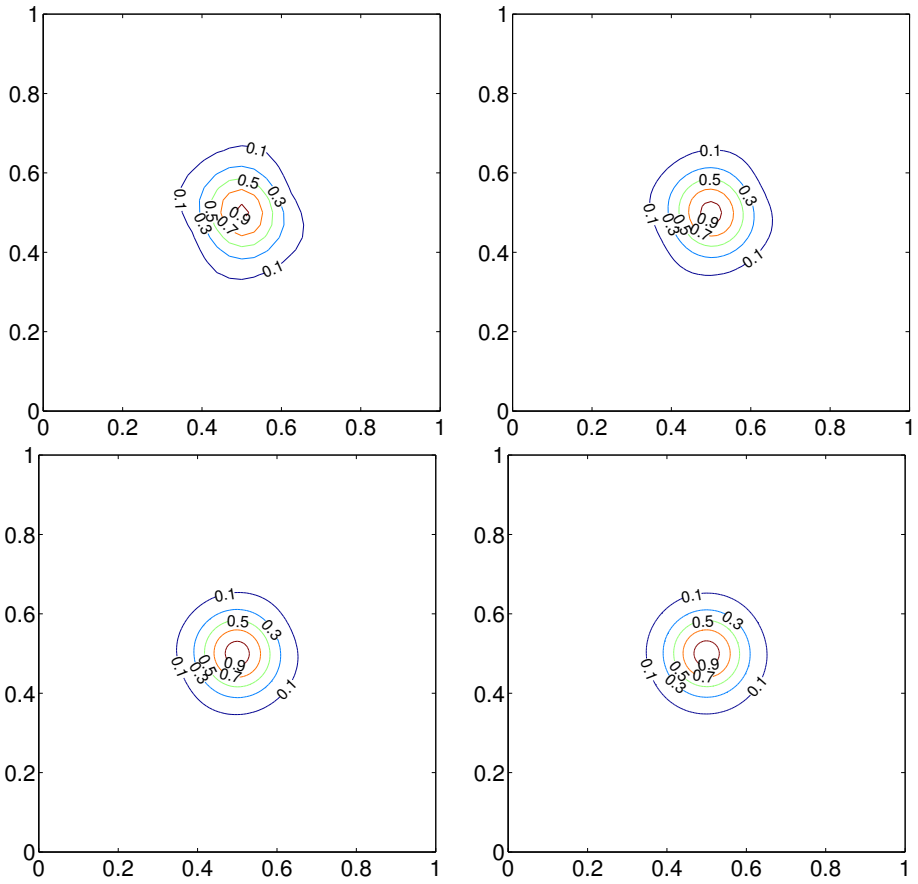

FIG. 6.4. *Example* 4: *The weak Galerkin solutions for mesh sizes* $h = 1/32$ *(top left),* $h = 1/48$ *(top right),* $h = 1/64$ *(bottom left), and* $h = 1/96$ *(bottom right).*

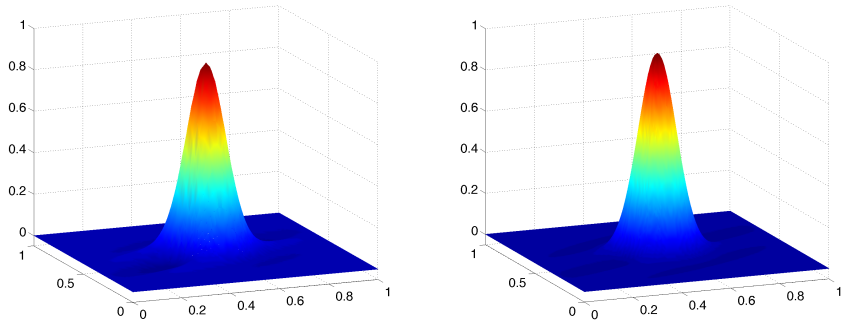

FIG. 6.5. *Example* 4: *The surface plots of the weak Galerkin solutions for mesh sizes* $h = 1/64$ *(left) and* $h = 1/96$ *(right).*

no oscillation. Figure 6.5 shows the surface plots for the corresponding numerical solutions for mesh sizes $h = 1/64$ and $h = 1/96$. No oscillation can be detected from either the surface or contour plots. Figure 6.6 illustrates the performance of the

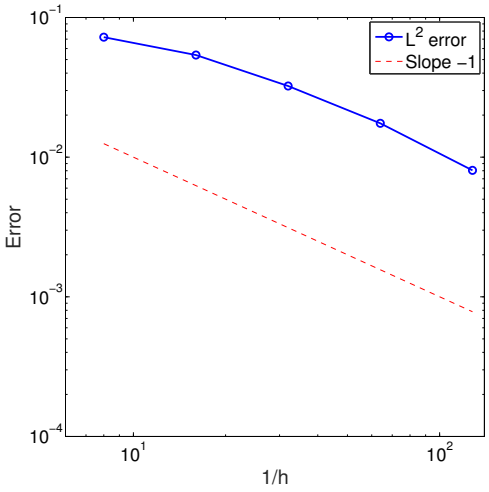

FIG. 6.6. *Example* 4: *The error plot in the* L^2*-norm.*

numerical method in the L^2-norm, which indicates a convergence at the rate of $\mathcal{O}(h)$ for this strongly anisotropic diffusion problem.

6.5. Example 5. This test problem also arises from the modeling of fluid flow in porous media with a strong anisotropic discontinuous permeability and a combination of point source and sinks that are viewed as Green's functions. The domain $\Omega = (0,1)^2$ is divided into four quadrants by the two lines $x = 1/2$ and $y = 1/2$. The permeability tensor is given by

$$a = \mathbf{K}_1 = \begin{pmatrix} 2464.36002 & 1148.68364 \\ 1148.68364 & 536.63998 \end{pmatrix} \tag{6.6}$$

in the first and third quadrants, whereas it takes the form

$$a = \mathbf{K}_2 = \begin{pmatrix} 2464.36002 & -1148.68364 \\ -1148.68364 & 536.63998 \end{pmatrix} \tag{6.7}$$

in the second and fourth quadrants.

Both $\mathbf{K}_1$ and $\mathbf{K}_2$ are strongly anisotropic, as the ratios of their eigenvalues are $1 : 3000$. Furthermore, the eigenvectors of $\mathbf{K}_1$ and $\mathbf{K}_2$ take different directions and hence generate strong discontinuity in permeability across the dividing lines. The two Gaussian sources are given by

$$f_1(x,y) = 10^5 \exp\left(- \frac{(x - x_c^{(1)})^2 + (y - y_c^{(1)})^2}{2\sigma^2} \right),$$
$$f_2(x,y) = -10^5 \exp\left(- \frac{(x - x_c^{(2)})^2 + (y - y_c^{(2)})^2}{2\sigma^2} \right),$$

where $(x_c^{(1)}, y_c^{(1)}) = (0.25, 0.25)$, $(x_c^{(2)}, y_c^{(2)}) = (0.75, 0.75)$, and $\sigma^2 = 0.05$.

These Gaussian sources are indeed concentrated in very small regions with values varying from near zero to the peak value of 10^5. We are not aware of any analytical solutions for this problem, but our numerical solutions can be compared with those

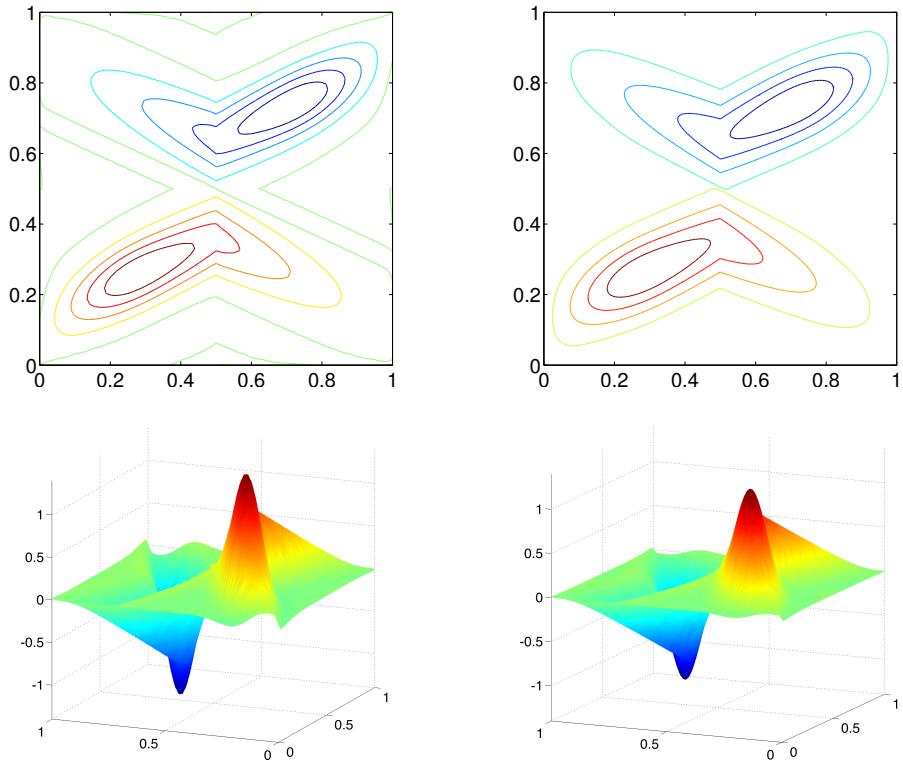

FIG. 6.7. *Example* 5: *The contour plots of the numerical solutions for mesh sizes* $h = 1/48$ *(top left) and* $h = 1/64$ *(top right); the surface plots of the numerical solutions for mesh sizes* $h = 1/48$ *(bottom left) and* $h = 1/64$ *(bottom right).*

presented in [21, 24]. Figure 6.7 shows the contour plots of the numerical solutions for mesh sizes $h = 1/48$ and $h = 1/64$ (top) and the surface plots of the same numerical solutions (bottom). The elliptic shape of the contours reflects the anisotropy in the permeability field. The discontinuity in permeability is also reflected in the plots. It can be seen that when the contours enter into the 4th quadrant from the 3rd one, deflection happens due to the change of the eigenvectors.

7. Numerical experiments for reaction-diffusion equations. The rest of the numerical experiments will be conducted for the following perturbed reaction-diffusion equation: Find an unknown function $u = u(x, y)$ satisfying

$$\begin{cases} -\epsilon^2 \Delta u + cu = f & \text{in } \Omega, \\ u = g & \text{on } \partial\Omega, \end{cases} \tag{7.1}$$

where $\epsilon > 0$ is a small parameter. The mixed formulation for (7.1) has the form

$$\begin{cases} \mathbf{q} + \nabla u = 0, \\ \epsilon^2 \nabla \cdot \mathbf{q} + cu = f. \end{cases}$$

As for the numerical scheme (2.2), the bilinear form $a(\cdot;\cdot)$ is given by

$$a(\boldsymbol{\tau}, w; \boldsymbol{\sigma}, v) = \sum_{T\in\mathcal{T}_h} \left((\epsilon^2\nabla_w\cdot\boldsymbol{\tau} + cw_0, \epsilon^2\nabla_w\cdot\boldsymbol{\sigma} + cv_0)_T + \epsilon^2(\boldsymbol{\tau}_0 + \nabla_w w, \boldsymbol{\sigma}_0 + \nabla_w v)_T\right) + \rho_1 s_1(w, v) + \rho_2 s_2(\boldsymbol{\tau}, \boldsymbol{\sigma}),$$

where $\rho_1 = \epsilon^2$ and $\rho_2 = \epsilon$. Our numerical experiments are based on the following selection of the finite element spaces:

$$V_h = \{v = \{v_0, v_b\} : \ v_0|_T \in P_1(T), v_b|_e \in P_1(e), e \subset \partial T\}$$

and

$$\Sigma_h = \{\boldsymbol{\sigma} = \{\boldsymbol{\sigma}_0, \boldsymbol{\sigma}_b\} : \ \boldsymbol{\sigma}_0|_T \in [P_0(T)]^d, \boldsymbol{\sigma}_b|_e = \sigma_b\mathbf{n}_e, \sigma_b|_e \in P_0(e), \ e \subset \partial T\}.$$

Note that the weak finite element functions for the boundary unknown u_b are constructed by using linear functions on each edge, which is different from constant functions as employed in previous test cases. It should be pointed out that the mathematical theory developed in the previous sections can be extended to this new combination without any difficulty. In this section, we shall numerically investigate the performance of the proposed numerical scheme.

The weak Galerkin least-squares finite element method then seeks $u_h \times \mathbf{q}_h \in V_h \times \Sigma_h$ satisfying $u_b = Q_b g$ on $\partial\Omega$ and

$$a(\mathbf{q}_h, u_h; \boldsymbol{\sigma}, v) = (f, \epsilon^2\nabla_w\cdot\boldsymbol{\sigma} + cv_0) \quad \forall \boldsymbol{\sigma} \times v \in \Sigma_h \times V_h^0. \tag{7.2}$$

In the case of $\epsilon \ll 1$, the reaction-diffusion equation (7.1) is known to be singularly perturbed, for which the solution has a boundary layer. The classical finite element method for singularly perturbed reaction-diffusion equations often produces numerical solutions with nonphysical oscillations. To overcome this difficulty, several advanced numerical techniques such as the Petrov–Galerkin, streamline upwinding [20], and adaptive meshing [33] have been developed in the last two decades.

The goal of this section is to numerically investigate the computational performance of the algorithm (2.2). The following ϵ-dependent norm shall be employed to measure the approximation property:

$$\|(e_h, \boldsymbol{\varepsilon}_h)\|_{1,\epsilon}^2 = a(\boldsymbol{\varepsilon}_h, e_h; \boldsymbol{\varepsilon}_h, e_h). \tag{7.3}$$

We shall numerically demonstrate that the numerical solution arising from (2.2) has the same order of convergence with respect to the norm (7.3) as the one reported in [26].

7.1. Example 6. Consider the reaction-diffusion problem

$$\begin{cases} -\epsilon^2 u'' + cu = f \text{ in } \Omega = (0,1), \\ u(0) = u(1) = 0, \end{cases} \tag{7.4}$$

where ϵ is a parameter to be specified in each test case, and f is computed such that the exact solution is given by

$$u(x) = x - \frac{e^{(x-1)/\epsilon} - e^{-(x+1)/\epsilon}}{1 - e^{-2/\epsilon}}.$$

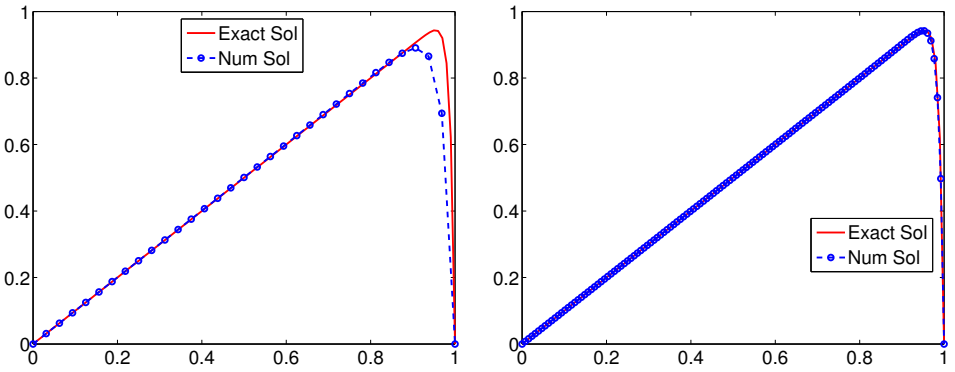

FIG. 7.1. *Example* 6: *The solution plots for* $\epsilon = 10^{-2}$ *for* $h = 1/32$ *(left) and* $h = 1/128$ *(right).*

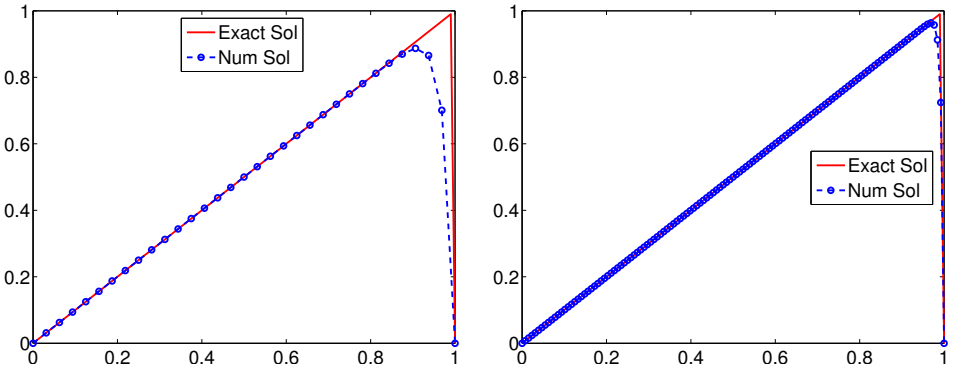

FIG. 7.2. *Example* 6: *The solution plots for* $\epsilon = 10^{-5}$ *for* $h = 1/32$ *(left) and* $h = 1/128$ *(right).*

This problem was used in [26]. For simplicity, we set $c(x) = 1$. Observe that the solution u has a boundary layer at $x = 1$.

The numerical solutions arising from the weak Galerkin least-squares finite element scheme (7.2) are shown in Figures 7.1 and 7.2 with $\epsilon = 10^{-2}$ and $\epsilon = 10^{-5}$ for mesh sizes $h = 1/32$ and $h = 1/128$. It can be seen that our numerical solutions do not have any oscillation, and they provide accurate approximations to the exact solution at the places away from the boundary layers. At or near the boundary layers, the weak Galerkin least-squares solution is accurate when the mesh size is small.

Table 7.1 illustrates the error and the order of convergence for the numerical scheme (7.2) measured in the ϵ-dependent norm (7.3) for the cases of $\epsilon = 1$, 10^{-1}, 10^{-2}, 10^{-3}, 10^{-4}, 10^{-5}, respectively. It can be observed that for $\epsilon = 1$ and $\epsilon = 10^{-1}$, the rates of convergence are both of optimal order at $O(h)$. However, when $\epsilon \ll h$, the problem becomes singularly perturbed and the theory developed in previous sections is not applicable. Nevertheless, our numerical experiments indicate that the weak Galerkin least-squares finite element scheme indeed converges, and the rate of convergence is $O(h^{0.5})$. This rate was considered as optimal in [25] for the singularly perturbed reaction-diffusion problems.

We also computed the error in some ϵ-independent norms. Figure 7.3 shows the total variation for the error function arising from the numerical scheme. It can be seen that the numerical solutions have bounded total variations for very small values of ϵ. Figure 7.4 illustrates the rate of convergence in the usual L^1-norm. For very small

TABLE 7.1
Example 6: *The rates of convergence for the different values of* ϵ.

	$h = 1/8$	$h = 1/16$	$h = 1/32$	$h = 1/64$	$h = 1/128$
ϵ=1	1.2852e-02	6.1062e-03	3.0118e-03	1.5007e-03	7.4968e-04
order		1.07	1.02	1.00	1.00
ϵ=1e-01	1.4275e-01	4.4912e-02	1.5586e-02	6.6189e-03	3.1450e-03
order		1.67	1.53	1.24	1.07
ϵ=1e-02	3.5481e-01	2.4215e-01	1.4166e-01	6.3093e-02	2.0685e-02
order		0.55	0.77	1.17	1.61
ϵ=1e-03	3.5357e-01	2.5006e-01	1.7694e-01	1.2541e-01	8.7531e-02
order		0.50	0.50	0.50	0.52
ϵ=1e-4	3.5355e-01	2.5000e-01	1.7678e-01	1.2500e-01	8.8401e-02
order		0.50	0.50	0.50	0.52
ϵ=1e-05	3.5357e-01	2.5006e-01	1.7678e-01	1.2500e-01	8.8388e-02
order		0.50	0.50	0.50	0.52

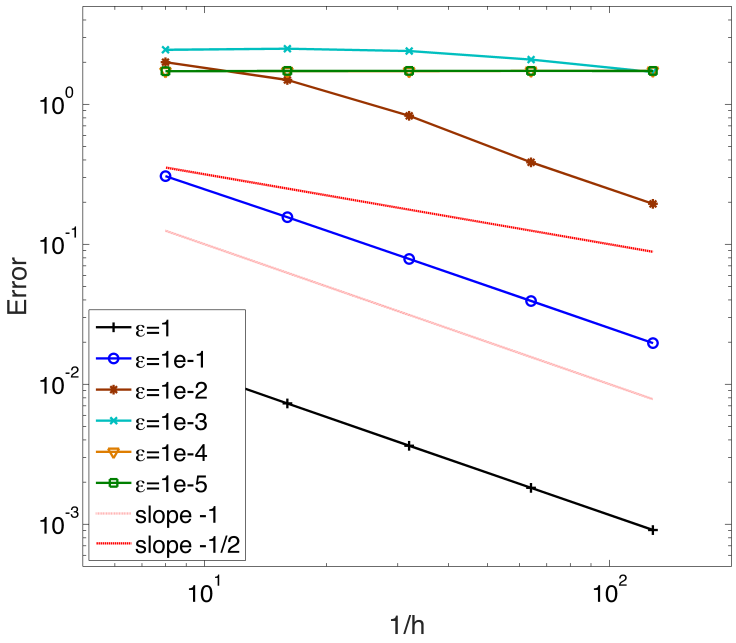

FIG. 7.3. *Example* 6: *The rates of convergence in the* $W^{1,1}$*-seminorm for* $\epsilon = 1$, 10^{-1}, 10^{-2}, 10^{-3}, 10^{-4}, *and* 10^{-5}.

values of ϵ, the numerical solutions are convergent at the rate of $\mathcal{O}(h)$ in the L^1-norm. Figure 7.5 demonstrates the convergence in the usual L^2-norm. The numerical results indicate that the error in L^2-norm exhibits a convergence property similar to that in the ϵ-dependent norm, namely, a convergence at the rate of $\mathcal{O}(h^{0.5})$ for small values of $\epsilon \ll h$.

7.2. Example 7. Consider again the one-dimensional reaction-diffusion equation (7.4) with a discontinuous coefficient $c(x)$ given by

$$c(x) = \begin{cases} 1 \text{ if } x < 0.5, \\ 2 - x \text{ if } x > 0.5. \end{cases}$$

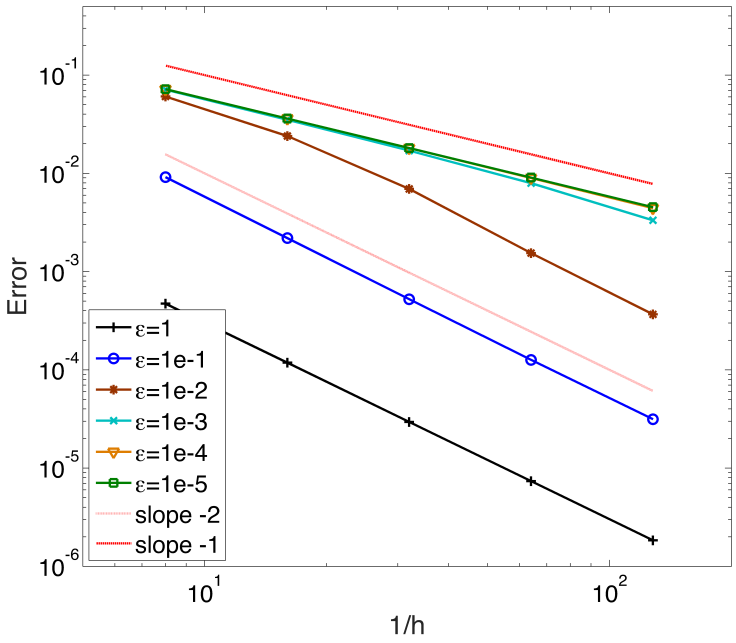

FIG. 7.4. *Example* 6: *The rates of convergence in the* L^1*-norm for* $\epsilon = 1$, 10^{-1}, 10^{-2}, 10^{-3}, 10^{-4}, *and* 10^{-5}.

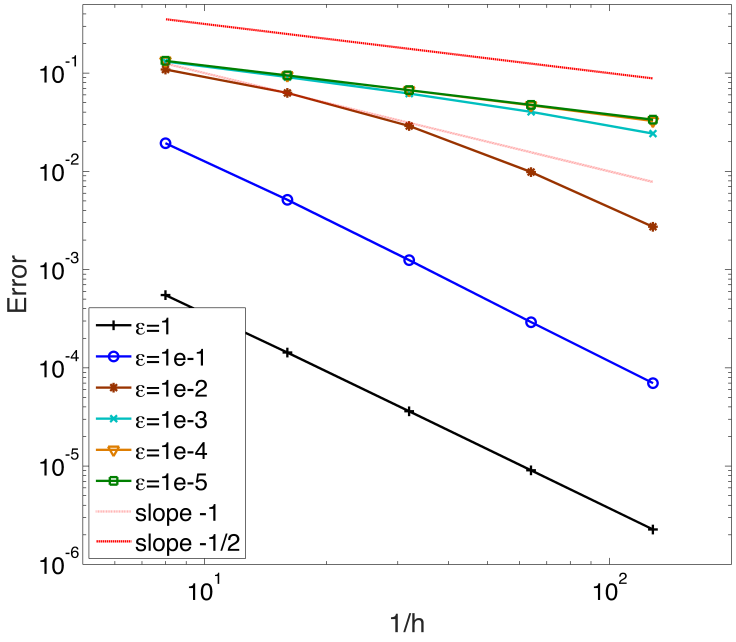

FIG. 7.5. *Example* 6: *The rates of convergence in the* L^2*-norm for* $\epsilon = 1$, 10^{-1}, 10^{-2}, 10^{-3}, 10^{-4}, *and* 10^{-5}.

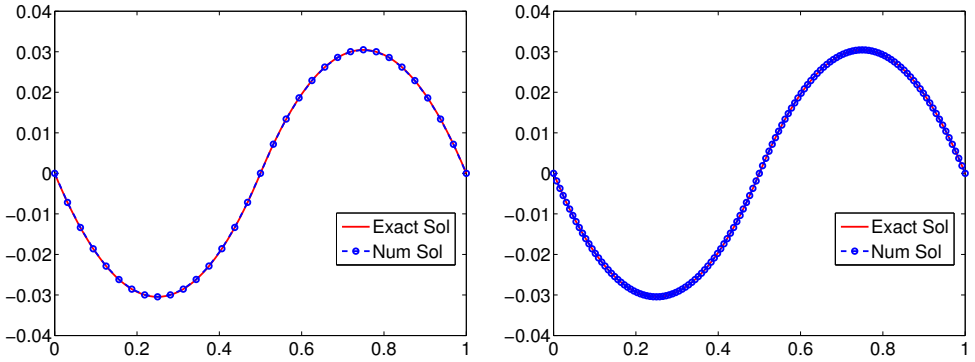

FIG. 7.6. *Example* 7: *The solution plots for* $\epsilon = 1$ *for* $h = 1/32$ *(left) and* $h = 1/128$ *(right).*

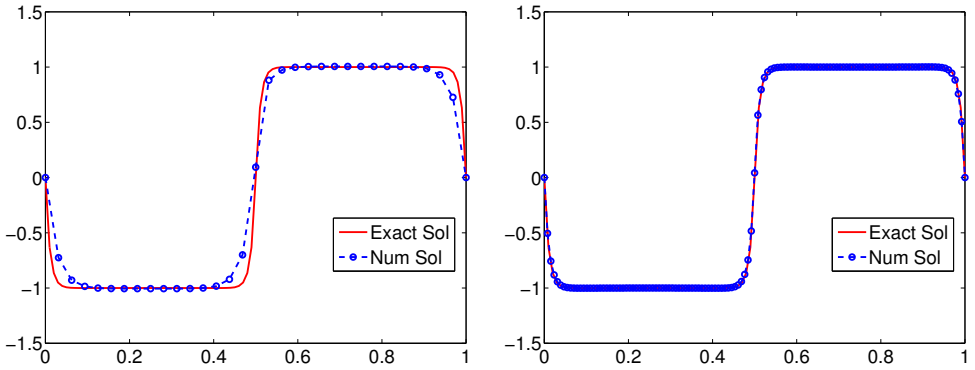

FIG. 7.7. *Example* 7: *The solution plots for* $\epsilon = 10^{-2}$ *for* $h = 1/32$ *(left) and* $h = 1/128$ *(right).*

The function f is computed so that the exact solution is

$$u(x) = \begin{cases} -1 + \dfrac{e^{-x/\epsilon} + e^{(2x-1)/(2\epsilon)}}{e^{-1/(2\epsilon)} + 1} & \text{if } x < 0.5, \\ 1 - \dfrac{e^{(x-1)/\epsilon} + e^{(1-2x)/(2\epsilon)}}{e^{-1/(2\epsilon)} + 1} & \text{if } x > 0.5. \end{cases}$$

The interface point $x = 0.5$ divides the domain $\Omega = (0, 1)$ into two subdomains: $\Omega_1 = (0, 0.5)$ and $\Omega_2 = (0.5, 1)$. Clearly, neither the coefficient c nor the load function f are continuous at the interface point $x = 0.5$. In fact, it is easy to see that u'' is discontinuous at this interface point, u has boundary layers at $x = 0$ and $x = 1$, and u has an interior layer at $x = 0.5$ when $\epsilon \ll 1$.

The weak Galerkin least-squares finite element scheme (7.2) was applied to this problem for $\epsilon = 1$, $\epsilon = 10^{-2}$, and $\epsilon = 10^{-5}$, respectively. The comparison of the interpolated exact solution and the numerical solution for the mesh size $h = 1/32$ for the various values of ϵ are plotted in Figures 7.6–7.8 (left). It can be seen that the numerical solutions do not possess any oscillations, and they provide accurate approximations at the places away from the interior or boundary layers. Finer meshes are necessary if one desires good approximations at the boundary layers.

In Table 7.2, we present some data on the error and the rate of convergence for the present test problem. For the case of $\epsilon = 1$, the test problem is well behaved

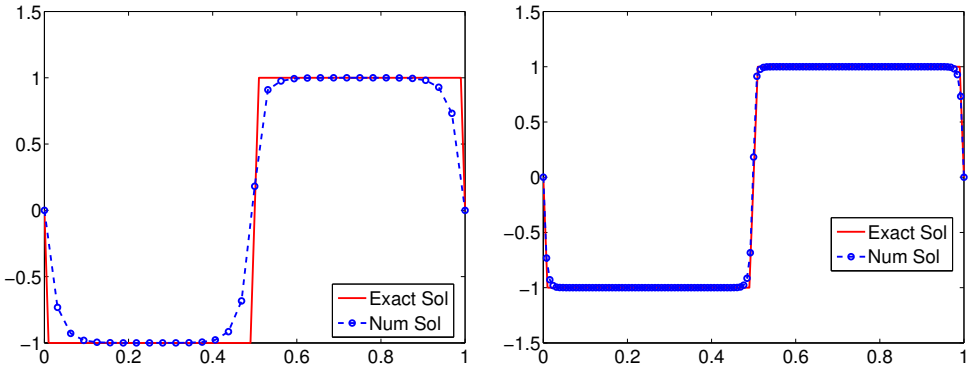

FIG. 7.8. *Example* 7: *The solution plots for* $\epsilon = 10^{-5}$ *for* $h = 1/32$ *(left) and* $h = 1/128$ *(right).*

TABLE 7.2
Example 7: *The rates of convergence for the different values of* ϵ.

	$h = 1/8$	$h = 1/16$	$h = 1/32$	$h = 1/64$	$h = 1/128$
ϵ=1	2.2343e-02	1.0924e-02	5.4294e-03	2.7095e-03	1.3538e-03
order		1.03	1.01	1.00	1.00
ϵ=1e-01	2.7385e-01	8.5127e-02	3.1298e-02	1.3830e-02	6.5927e-03
order		1.69	1.44	1.18	1.07
ϵ=1e-02	7.1782e-01	4.8657e-01	2.8132e-01	1.2174e-01	3.8715e-02
order		0.56	0.79	1.21	1.65
ϵ=1e-03	7.2343e-01	5.1244e-01	3.6216e-01	2.5547e-01	1.7678e-01
order		0.50	0.50	0.50	0.50
ϵ=1e-04	7.2422e-01	5.1362e-01	3.6369e-01	2.5723e-01	1.8176e-01
order		0.50	0.50	0.50	0.50
ϵ=1e-05	7.2427e-01	5.1370e-01	3.6382e-01	2.5746e-01	1.8211e-01
order		0.50	0.50	0.50	0.50

so that the optimal order of convergence is expected. For $\epsilon = 10^{-5}$, the problem is singularly perturbed, and our numerical experiments indicate that the error measured in the norm defined in (7.3) is decreasing at the optimal rate of $O(h^{0.5})$, as observed in [27, 34] for the singularly perturbed problems.

Figure 7.9 illustrates the weak Galerkin least-squares solutions with a stabilizing parameter of $\rho_2 = \epsilon^2$. For this selection of ρ_2, we observed some oscillation or overshooting of the numerical solution around the interface point $x = 0.5$. As the mesh size is reduced from $h = 1/32$ to $h = 1/128$, we see a slight reduction in the oscillation, but the overshooting stays unchanged. This experiment shows that the choice of the stabilizing parameter plays an important role in the weak Galerkin least-squares finite element method for singularly perturbed problems. More research should be conducted regarding the impact of the stabilizer in the algorithm design and analysis.

7.3. Example 8. Consider the reaction-diffusion problem (7.1) in two dimensions with $c = 1 + x^2y^2e^{xy/2}$. The load function f and the Dirichlet boundary values are chosen so that the exact solution is given by

$$u = x^3(1+y^2) + \sin(\pi x^2) + \cos(\pi y/2) \\ + (x+y)[e^{-2x/\epsilon} + e^{-2(1-x)/\epsilon} + e^{-3y/\epsilon} + e^{-3(1-y)/\epsilon}].$$

In the weak Galerkin scheme (7.2), the two stabilizing parameters are set as $\rho_1 =$

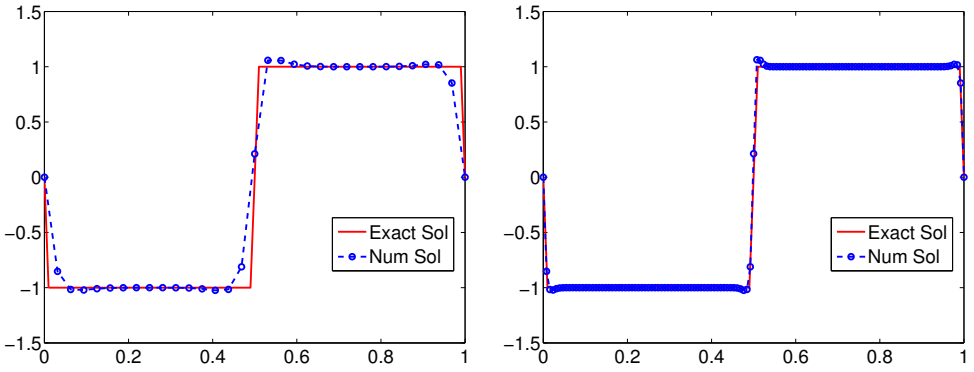

FIG. 7.9. *Example* 7: *The solution plots for* $\epsilon = 10^{-5}$, $\rho_1 = \epsilon^2$, *and* $\rho_2 = \epsilon^2$ *for* $h = 1/32$ *(left) and* $h = 1/128$ *(right).*

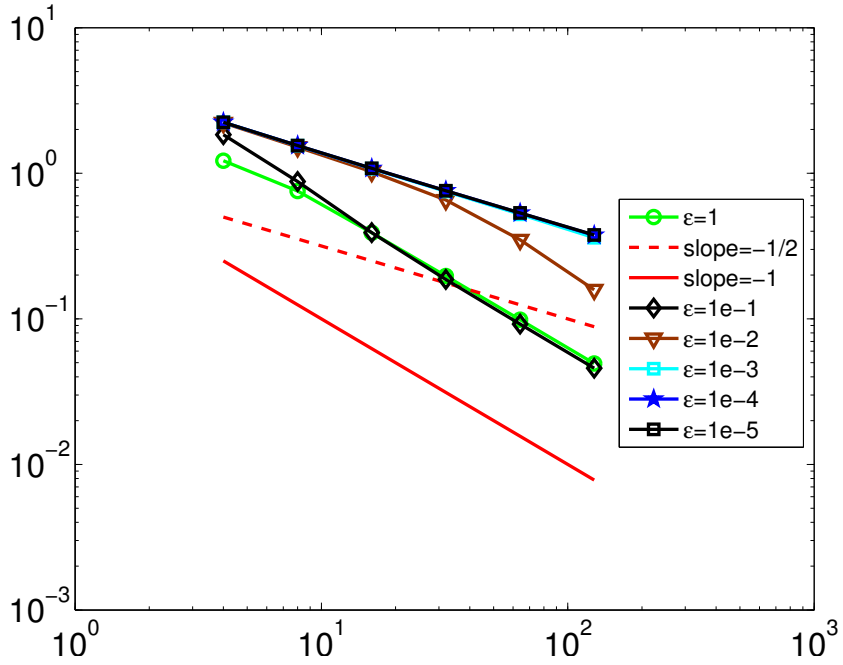

FIG. 7.10. *Example* 8: *The rates of convergence in an* ϵ*-dependent norm for* $\epsilon = 1, 10^{-1}, 10^{-2}, 10^{-3}, 10^{-4}$, *and* 10^{-5}.

ϵ^2 and $\rho_2 = \epsilon$. Figure 7.10 illustrates the rates of convergence for the corresponding numerical solutions in the ϵ-dependent norm (7.3) for the test cases with $\epsilon = 1$, $\epsilon = 10^{-1}$, $\epsilon = 10^{-2}$, $\epsilon = 10^{-3}$, $\epsilon = 10^{-4}$, and $\epsilon = 10^{-5}$. For the cases of $\epsilon = 1$ and $\epsilon = 10^{-1}$, the numerical solutions converge at the optimal rate of $O(h)$. When ϵ is small (say, $\epsilon = 10^{-5}$), the error converges uniformly in ϵ with an order $O(h^{0.5})$. The weak Galerkin least-square finite element solution and the exact solution for $\epsilon = 10^{-5}$ and $h = 1/128$ are plotted in Figure 7.11. The numerical solution is accurate at the places away from the three corner points $(0, 1), (1, 0)$, and $(1, 1)$ where the exact solution is singular. In fact, the singularity is so strong that the solution changes very

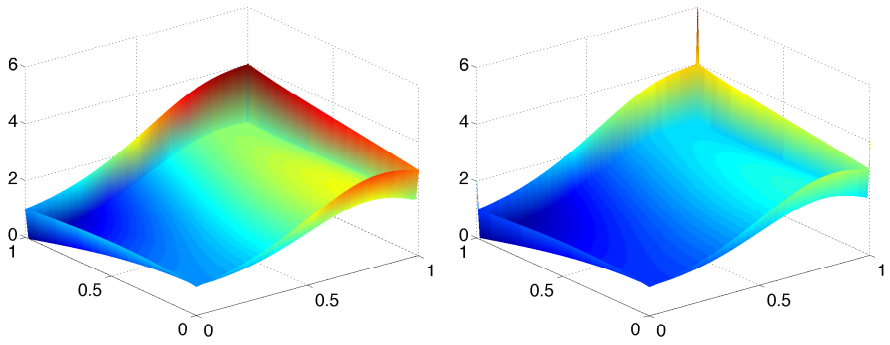

FIG. 7.11. *Example* 8: *For* $h = 1/128$ *and* $\epsilon = 10^{-5}$, *the weak Galerkin solution (left) and the exact solution (right).*

rapidly when moving away from the corners. For example, it can be computed that $u(1,1) = 6$, while $u(1, 0.99) = 3.9858$, $u(1, 0.999) = 3.9986$, and $u(0.999, 1) = 3.9993$. We believe that very fine meshes are needed around these three corner points in order to resolve the strong singularities.

Acknowledgment. The authors would like to offer their gratitude to Professor Zhiqiang Cai for his helpful discussion on the least-squares finite element methods.

REFERENCES

[1] D. N. ARNOLD, F. BREZZI, B. COCKBURN, AND L. D. MARINI, *Unified analysis of discontinuous Galerkin methods for elliptic problems*, SIAM J. Numer. Anal., 39 (2002), pp. 1749–1779, https://doi.org/10.1137/S0036142901384162.

[2] L. VEIGA, K. LIPNIKOV, AND G. MANZINI, *Convergence analysis of the high-order mimetic finite difference method*, Numer. Math., 113 (2009), pp. 325–356.

[3] P. BOCHEV AND M. GUNZBURGER, *Accuracy of the least squares methods for the Navier Stokes equations*, Comput. Fluids, 22 (1993), pp. 549–563.

[4] P. B. BOCHEV AND M. D. GUNZBURGER, *Analysis of least-squares finite element methods for the Stokes equations*, Math. Comp., 63 (1994), pp. 479–506.

[5] P. BOCHEV AND M. GUNZBURGER, *Least-Squares Finite Element Methods*, Springer, New York, 2009.

[6] P. BOCHEV, J. LAI, AND L. OLSON, *A locally conservative, discontinuous least-squares finite element method for the Stokes equations*, Internat. J. Numer. Methods Fluids, 68 (2011), pp. 782–804.

[7] P. BOCHEV, J. LAI, AND L. OLSON, *A non-conforming least-squares finite element method for the velocity-vorticity-pressure Stokes equations*, Internat. J. Numer. Methods Fluids, 00 (2011), pp. 1–19.

[8] D. BOFFI, F. BREZZI, AND M. FORTIN, *Mixed Finite Element Methods and Applications*, Springer, Heidelberg, 2013.

[9] D. BOFFI, M. BOTTI, AND A. DI PIETRO, *A nonconforming high-order method for the Biot problem on general meshes*, SIAM J. Sci. Comput., 38 (2016), pp. A1508–A1537, https://doi.org/10.1137/15M1025505.

[10] J. BRAMBLE, R. LAZAROV, AND J. PASCIAK, *A least-squares approach based on a discrete minus one inner product for first order systems*, Math. Comp., 66 (1997), pp. 935–955.

[11] Z. CAI AND X. YE, *A least-squares finite element approximation for the compressible Stokes equations*, Numer. Methods Partial Differential Equations, 16 (2000), pp. 62–70.

[12] Z. CAI, X. YE, AND H. ZHANG, *Least-squares finite element approximations for the Reissner-Mindlin plate*, Numer. Linear Algebra Appl., 6 (1999), pp. 479–496.

[13] Z. CAI, R. LAZAROV, T. A. MANTEUFFEL, AND S. F. MCCORMICK, *First-order system least squares for second-order partial differential equations: Part* I, SIAM J. Numer. Anal., 31 (1994), pp. 1785–1799, https://doi.org/10.1137/0731091.

[14] Z. Cai, T. A. Manteuffel, and S. F. McCormick, *First-order system least squares for second-order partial differential equations: Part* II, SIAM J. Numer. Anal., 34 (1997), pp. 425–454, https://doi.org/10.1137/S0036142994266066.
[15] C. L. Chang, *An error estimate of the least squares finite element methods for the Stokes problem in three dimensions*, Math. Comp., 63 (1994), pp. 41–50.
[16] B. Cockburn, J. Gopalakrishnan, and R. Lazarov, *Unified hybridization of discontinuous Galerkin, mixed, and continuous Galerkin methods for second order elliptic problems*, SIAM J. Numer. Anal., 47 (2009), pp. 1319–1365, https://doi.org/10.1137/070706616.
[17] B. Cockburn and C.-W. Shu, *The local discontinuous Galerkin method for time-dependent convection-diffusion systems*, SIAM J. Numer. Anal., 35 (1998), pp. 2440–2463, https://doi.org/10.1137/S0036142997316712.
[18] L. Demkowicz and J. Gopalakrishnan, *Analysis of the DPG method for the Poisson equation*, SIAM J. Numer. Anal., 49 (2011), pp. 1788–1809, https://doi.org/10.1137/100809799.
[19] L. Demkowicz and J. Gopalakrishnan, *A primal DPG method without a first order reformulation*, Comput. Math. Appl., 66 (2013), pp. 1058–1064.
[20] L. Demkowicz and I. Harari, *Robust Discontinuous Petrov Galerkin (DPG) Methods for Reaction Dominated Diffusion*, ICES REPORT 14-36, Institute for Computational Engineering and Sciences, The University of Texas at Austin, Austin, TX, 2014.
[21] M. Edwards and H. Zheng, *A quasi-positive family of continuous Darcy-flux finite-volume schemes with full pressure support*, J. Comput. Phys., 227 (2008), pp. 9333–9364.
[22] B. Jiang and L. Povinelli, *Optimal least-squares finite element method for elliptic problems*, Comput. Methods. Appl. Mech. Engrg., 102 (1993), pp. 199–212.
[23] B. Jiang and L. Povinelli, *Least-squares finite element method for fluid dynamics*, Comput. Methods Appl. Mech. Engrg., 81 (1990), pp. 13–37.
[24] G. Lin, J. Liu, L. Mu, and X. Ye, *Weak Galerkin finite element methods for Darcy flow: Anisotropy and heterogeneity*, J. Comput. Phys., 276 (2014), pp. 422–437.
[25] R. Lin, *A robust finite element method for singularly perturbed convection-diffusion problems*, Discrete Contin. Dyn. Syst., (2009), pp. 496–505.
[26] R. Lin, *Discontinuous discretization for least-squares formulation of singularly perturbed reaction-diffusion problems in one and two dimensions*, SIAM J. Numer. Anal., 47 (2008), pp. 89–108, https://doi.org/10.1137/070700267.
[27] R. Lin, *Discontinuous Galerkin least-squares finite element methods for singularly perturbed reaction-diffusion problems with discontinuous coefficients and boundary singularities*, Numer. Math., 112 (2009), pp. 295–318.
[28] T. A. Manteuffel, S. F. McCormick, J. G. Schmidt, and C. R. Westphal, *First-order system least squares for geometrically nonlinear elasticity*, SIAM J. Numer. Anal., 44 (2006), pp. 2057–2081, https://doi.org/10.1137/050628027.
[29] L. Mu, J. Wang, and X. Ye, *A Weak Galerkin finite element method with polynomial reduction*, J. Comput. Appl. Math., 285 (2015), pp. 45–58.
[30] A. I. Pehlivanov, G. F. Carey, and R. D. Lazarov, *Least-squares mixed finite elements for second-order elliptic problems*, SIAM J. Numer. Anal., 31 (1994), pp. 1368–1377, https://doi.org/10.1137/0731071.
[31] D. Pietro and A. Ern, *A hybrid high-order locking-free method for linear elasticity on general meshes*, Comput. Methods Appl. Mech. Engrg., 283 (2015), pp. 1–21.
[32] D. Pietro and A. Ern, *Hybrid high-order methods for variable-diffusion problems on general meshes*, C. R. Math. Acad. Sci. Paris, 353 (2015), pp. 31–34.
[33] H. Roos, *Layer-adapted grids for singular perturbation problems*, ZAMM Z. Angew. Math. Mech., 78 (1998), pp. 291–309.
[34] H. Roos, *A note on the conditioning of upwind schemes on Shishkin meshes*, IMA J. Numer Anal., 16 (1996), pp. 529–538.
[35] L. Veiga, F. Brezzi, A. Cangiani, G. Manzini, L. Marini, and A. Russo, *Basic principles of virtual element methods*, Math. Models Methods Appl. Sci., 23 (2013), pp. 119–214.
[36] J. Wang and X. Ye, *A weak Galerkin finite element method for second order elliptic problems*, J. Comput. Appl. Math., 241 (2013), pp. 103–115.
[37] J. Wang and X. Ye, *A weak Galerkin mixed finite element method for second-order elliptic problems*, Math. Comp., 83 (2014), pp. 2101–2126.